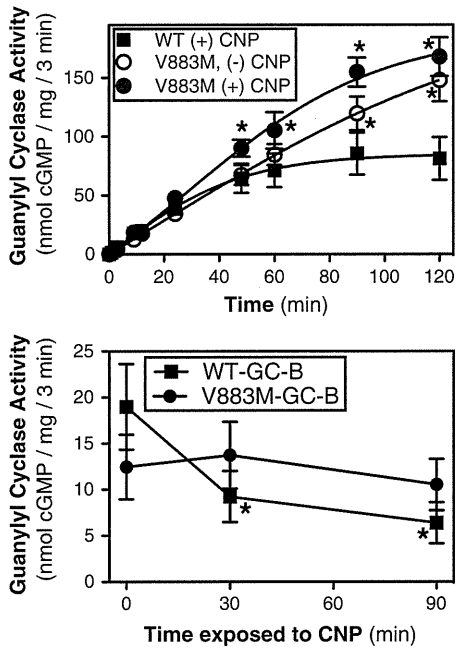

Fig. 4. V883M-GC-B is resistant to desensitization. A. GC assays were conducted on crude membranes from 293 cells transfected with HA-WT-GC-B or HA-V883M-GC-B for the period of time indicated in the presence of 1 mM GTP, 1 mM ATP and 5 mM $Mg^{2+}Cl_2$ with or without 1 μM CNP. Each value represents 4 determinations. The asterisks indicate a significant difference from corresponding values obtained in membranes expressing WT-GC-B at $p < 0.02$. B. Whole 293 cells transfected with HA-WT-GC-B or HA-V883M-GC-B were incubated with 1 μM CNP for the indicated times. Membranes were then prepared and assayed for GC activity in the presence of 1 mM GTP, 1 mM ATP and 5 mM $Mg^{2+}Cl_2$. N = 4. The asterisks indicate significance from the 0 time point value where $p < 0.05$. The bars within the symbols indicate SEM in all panels.

presence of CNP, whereas mutant activity was determined in the presence and absence of CNP. The GC activity of the WT enzyme declined with time and was inactive after 60 min. In contrast, the GC activity of the mutant receptor was linear for the duration of the assay regardless of whether CNP was included in the assay.

We also examined the inactivation of the WT and mutant enzymes under whole cell conditions. In this experiment, intact cells were treated with 1 μM CNP for 0, 30 or 90 min then membranes were prepared from the cells and assayed for GC activity for 3 min (Fig. 4, bottom panel). The WT enzyme demonstrated a time-dependent inactivation similar to that previously reported for GC-B expressed in 3T3 cells [8]. However, exposure of the V883M-GC-B to saturating concentrations of CNP failed to inactivate the enzyme after 30 or 90 min. Together, these data indicate that the Val substitution at position 883 not only increases the maximal velocity of the enzyme, it also disrupts the normal desensitization process.

Activation of GC-B by the V883M substitution does not require phosphorylation

CNP only activated a GC-B construct containing alanine substitutions for the first six phosphorylation sites identified in GC-B (S513, T516, S518, S523, S526, T529) two-fold as opposed to greater than 30-fold for WT-GC-B [29], whereas the analogous substitutions left GC-A completely unresponsive to NP stimulation [38]. These observations led to the idea that phosphorylation is required for NP-dependent activation of GC-A and GC-B. Here, we asked whether phosphorylation is also required for the V883M mutation to increase GC-B activity.

To do this, we mutated Val-883 to Met in the rat GC-B-7A construct that contains alanine substitutions for the first six identified sites plus Ser-522, which is not phosphorylated [29]. We also created a constitutively phosphorylated mimetic version of rat GC-B-V883M by mutating Val-883 to Met in GC-B-7E. Rat GC-B-7E contains glutamate substitutions for the first six identified sites as well as Ser-489, a newly identified putative site that reduces the Km of GC-B when phosphorylated [30].

Introducing the Val-883–Met mutation into WT-GC-B increased basal activity 39-fold, whereas the same mutation in the dephosphorylated form of the enzyme (GC-B-7A) increased activity 17-fold (Fig. 5). However, introduction of the V883M mutation into the GC-B-7E construct increased activity 68-fold. Thus, phosphorylation is not required for the elevated basal activity associated with the V883M mutation, but phosphorylation results in greater activation since the WT and phosphorylation mimetic enzymes (GC-B-7E) were activated to a greater degree than the non-phosphorylated enzyme (GC-B-7A).

Discussion

Characterization of the missense mutant revealed several important changes in GC-B that occurred as a result of this single amino acid substitution. First, basal maximal velocity was dramatically increased. Second, the CNP-dependent reduction in Km was rendered independent of ATP, and thirdly, the normal desensitization process was inactivated. Another worthy point of discussion is that the V883M-GC-B mutant is the first example of a GC where ligand binding reduces the Km without increasing maximal velocity. Thus, the kinetic analysis of this mutant allowed the separation of the maximal velocity increasing effects of ligand binding from the Km reducing effects of ligand binding for the first time. This mutant enzyme also provides unequivocal support for the new GC-B activation model where CNP binding increases activity by reducing the Km as well as increasing maximal velocity [6].

Early studies indicated that product formation by membrane GCs in the presence of detergent is positive cooperative [39,40]. We found that GC-B is positive cooperative under basal conditions as well as when assayed in the presence of Mn^{2+}GTP and Triton X-100. However, the single V883M mutation converts the enzyme from positive cooperative to slightly negative cooperative when assayed under both physiologic and detergent-activated conditions. Interestingly, CNP increased the degree of negative cooperativity of V883M-GC-B in a concentration-dependent manner.

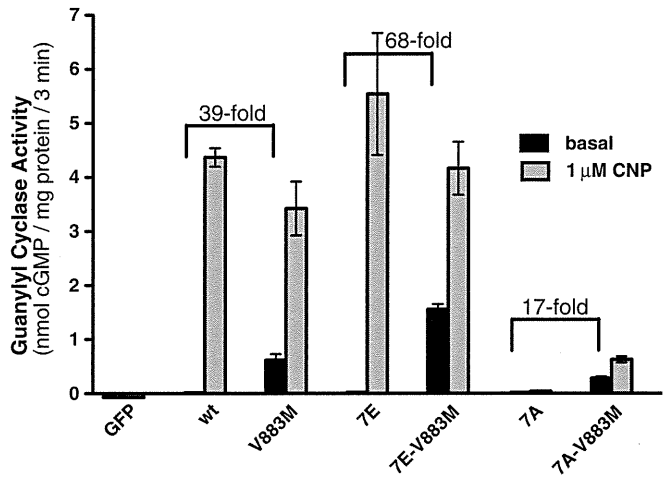

Fig. 5. The GC-B-V883M mutation activates a dephosphorylated version of GC-B. The V883M mutation was introduced into WT-GC-B, constitutively phosphorylated (7E) or constitutively dephosphorylated (7A) forms of GC-B. 293 cells were transiently transfected with plasmids expressing the indicated GC-B constructs. GC assays were performed for 3 min in the presence of 0.1 mM GTP, 1 mM ATP and 5 mM $Mg^{2+}Cl_2$ with or without 1 μM CNP. Each value represents 6 determinations. The bars within the symbols indicate SEM. The values above the brackets indicate the fold-difference above basal values.

The reduction in Km and increase in negative cooperativity appear paradoxical. We hypothesize that the V883M mutant locks the enzyme into a conformation that mimics an ATP bound state. This hypothesis is supported by low or no cooperativity under basal conditions and the inability of ATP to change the activity of the mutant enzyme. In addition, CNP alone markedly decreased the Km of GC-B-V883M, a phenomenon that requires ATP with the WT enzyme. Since cooperativity is maintained, this suggests that the mutation does not destroy the ability of GTP to bind to the allosteric site but rather modifies how GTP binding to the allosteric site affects the catalytic site. However, an alternative

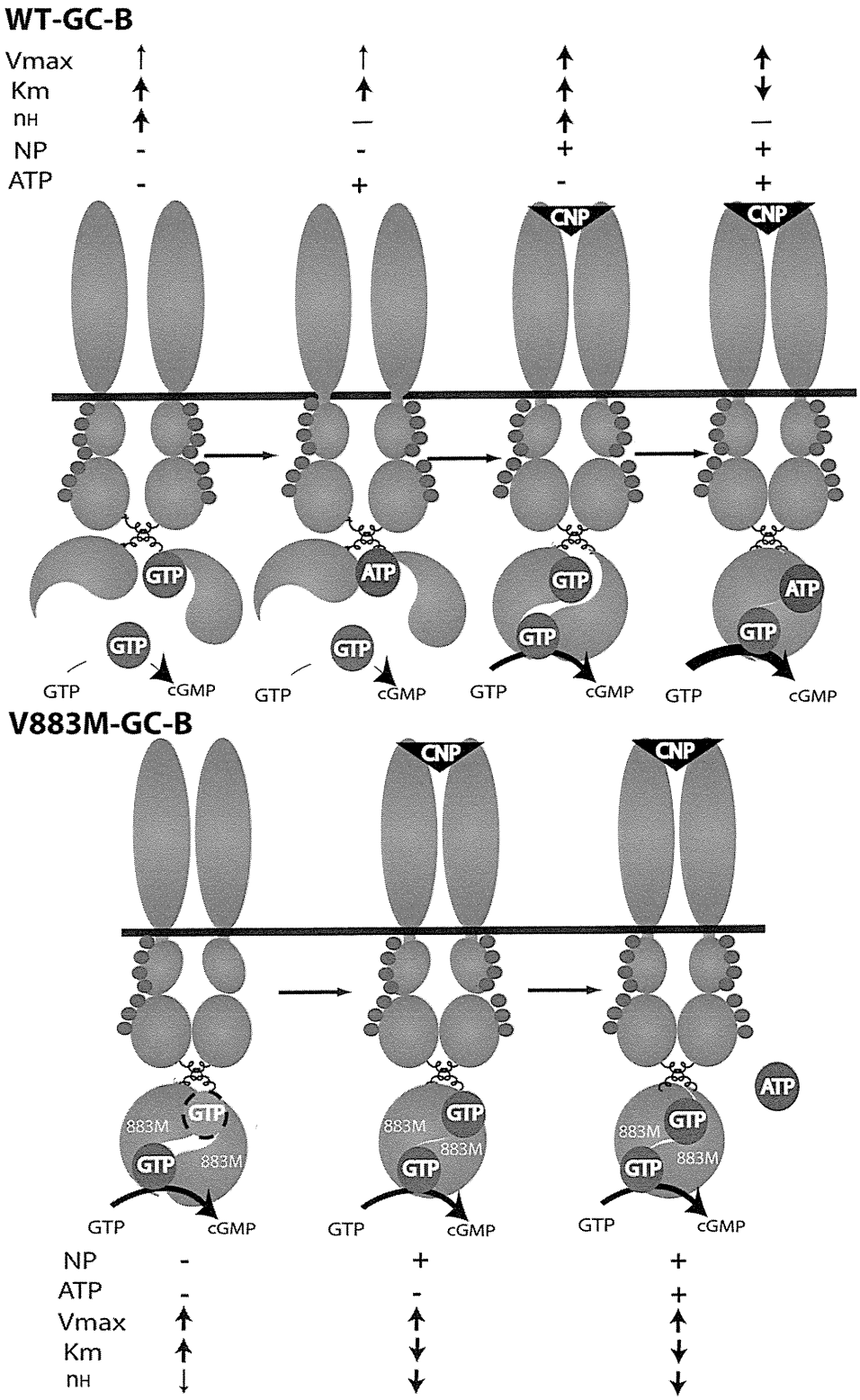

Fig. 6. Activation models for wild type and mutant GC-B. The models are described in detail under the Discussion section. The blue spheres indicate known phosphorylation sites in the kinase homology domain of GC-B. The white 883M indicates that the Val to Met mutation is in the catalytic domain. The abbreviations are: CNP, C-type natriuretic peptide; Km, Michaelis constant; n_H, Hill coefficient; and Vmax, maximal velocity.

explanation is that the reduction in the Hill coefficient results from increased inhibition resulting from GTP binding to a site independent of the allosteric site. This third GTP binding site would explain the appearance of negative cooperativity while also allowing for the Km reduction resulting from the previously identified allosteric site. It is also possible that the V883M mutation could increase the affinity of GC-B for the products of the reaction (pyrophosphate and cGMP), which would result in reduced GC activity and apparent negative cooperativity. Importantly, since the V883M mutation did not affect Vmax when measured in the presence of detergent and manganese, it suggests that the mutation modifies the conformation of the active site under physiologic conditions and does not directly interact with the substrate.

Near linear cGMP production with time by HA-V883M-GC-B assayed both in the presence and absence of CNP indicated that HA-V883M-GC-B is resistant to desensitization. Experiments with alanine and glutamate substituted receptors indicated that unlike CNP activation of WT-GC-B, the increased activity observed with the V883M mutation does not require phosphorylation of the kinase homology domain, although activation was greater with the phosphorylated and phosphomimetic enzymes. The lack of dependence on phosphorylation for activity of the mutant enzyme may contribute to its resistance to desensitization.

It is surprising how much the single amino acid substitution changes the regulation of GC-B (Fig. 6). In the absence of CNP and ATP, maximal velocity of WT-GC-B was low, affinity for substrate was low (high Km), and cooperative was significant and positive. In contrast, under the same conditions, maximal velocity of V883M-GC-B was high, affinity for substrate was low, and cooperativity was low and negative. Addition of ATP in the absence of CNP abolished positive cooperativity of the WT enzyme due to ATP replacing GTP at the allosteric site [6], but had no effect on the mutant enzyme under identical conditions. CNP alone increased maximal velocity of the WT enzyme, but it did not decrease the Km in the absence of ATP. In contrast, CNP alone failed to increase maximal velocity of the mutant enzyme but decreased the Km ten-fold in the absence of ATP. Finally, CNP reduced the cooperativity of both enzymes, but the WT enzyme went from positive to no cooperativity, whereas the mutant went from slightly negative cooperative to very negative cooperative.

In conclusion, we established a molecular mechanism for how a single amino acid substitution in GC-B activates the enzyme, which results in abnormally long and fragile human bones. It will be interesting to determine the prevalence of this mutation in humans and other species.

Conflict of interest statement

None of the authors have a conflict of interest associated with this study.

Acknowledgments

Grant-in Aid (21,922) from the University of Minnesota Graduate School to LRP and the National Institute of Arthritis and Musculoskeletal and Skin Diseases Training Grant T32AR050938 to JWR supported this work.

References

[1] Tamura N, Doolittle LK, Hammer RE, Shelton JM, Richardson JA, Garbers DL. Critical roles of the guanylyl cyclase B receptor in endochondral ossification and development of female reproductive organs. Proc Natl Acad Sci U S A 2004;101:17300–5.
[2] Schmidt H, Stonkute A, Juttner R, Schaffer S, Buttgereit J, Feil R, et al. The receptor guanylyl cyclase Npr2 is essential for sensory axon bifurcation within the spinal cord. J Cell Biol 2007;179:331–40.
[3] Zhang M, Su YQ, Sugiura K, Xia G, Eppig JJ. Granulosa cell ligand NPPC and its receptor NPR2 maintain meiotic arrest in mouse oocytes. Science 2010;330:366–9.
[4] Potter LR, Hunter T. Guanylyl cyclase-linked natriuretic peptide receptors: structure and regulation. J Biol Chem 2001;276:6057–60.
[5] Antos LK, Potter LR. Adenine nucleotides decrease the apparent Km of endogenous natriuretic peptide receptors for GTP. Am J Physiol Endocrinol Metab 2007;293:E1756–63.
[6] Robinson JW, Potter LR. Guanylyl cyclases A and B are asymmetric dimers that are allosterically activated by ATP binding to the catalytic domain. Sci Signal 2012;5:ra65.
[7] Duda T, Goraczniak RM, Sitaramayya A, Sharma RK. Cloning and expression of an ATP-regulated human retina C-type natriuretic factor receptor guanylate cyclase. Biochemistry 1993;32:1391–5.
[8] Potter LR. Phosphorylation-dependent regulation of the guanylyl cyclase-linked natriuretic peptide receptor B: dephosphorylation is a mechanism of desensitization. Biochemistry 1998;37:2422–9.
[9] Hagiwara H, Sakaguchi H, Itakura M, Yoshimoto T, Furuya M, Tanaka S, et al. Autocrine regulation of rat chondrocyte proliferation by natriuretic peptide C and its receptor, natriuretic peptide receptor-B. J Biol Chem 1994;269:10729–33.
[10] Suda M, Ogawa Y, Tanaka K, Tamura N, Yasoda A, Takigawa T, et al. Skeletal overgrowth in transgenic mice that overexpress brain natriuretic peptide. Proc Natl Acad Sci U S A 1998;95:2337–42.
[11] Krejci P, Masri B, Fontaine V, Mekikian PB, Weis M, Prats H, et al. Interaction of fibroblast growth factor and C-natriuretic peptide signaling in regulation of chondrocyte proliferation and extracellular matrix homeostasis. J Cell Sci 2005;118:5089–100.
[12] Woods A, Khan S, Beier F. C-type natriuretic peptide regulates cellular condensation and glycosaminoglycan synthesis during chondrogenesis. Endocrinology 2007;148:5030–41.
[13] Chusho H, Tamura N, Ogawa Y, Yasoda A, Suda M, Miyazawa T, et al. Dwarfism and early death in mice lacking C-type natriuretic peptide. Proc Natl Acad Sci U S A 2001;98:4016–21.
[14] Tamura N, Garbers DL. Regulation of the guanylyl cyclase-B receptor by alternative splicing. J Biol Chem 2003;278:48880–9.
[15] Jaubert J, Jaubert F, Martin N, Washburn LL, Lee BK, Eicher EM, et al. Three new allelic mouse mutations that cause skeletal overgrowth involve the natriuretic peptide receptor C gene (Npr3). Proc Natl Acad Sci U S A 1999;96:10278–83.
[16] Matsukawa N, Grzesik WJ, Takahashi N, Pandey KN, Pang S, Yamauchi M, et al. The natriuretic peptide clearance receptor locally modulates the physiological effects of the natriuretic peptide system. Proc Natl Acad Sci U S A 1999;96:7403–8.
[17] Tamura N, Ogawa Y, Chusho H, Nakamura K, Nakao K, Suda M, et al. Cardiac fibrosis in mice lacking brain natriuretic peptide. Proc Natl Acad Sci U S A 2000;97:4239–44.
[18] Kake T, Kitamura H, Adachi Y, Yoshioka T, Watanabe T, Matsushita H, et al. Chronically elevated plasma C-type natriuretic peptide level stimulates skeletal growth in transgenic mice. Am J Physiol Endocrinol Metab 2009;297:E1339–48.
[19] Lorget F, Kaci N, Peng J, Benoist-Lasselin C, Mugniery E, Oppeneer T, et al. Evaluation of the therapeutic potential of a CNP analog in a Fgfr3 mouse model recapitulating achondroplasia. Am J Hum Genet 2012;91:1108–14.
[20] Yasoda A, Kitamura H, Fujii T, Kondo E, Murao N, Miura M, et al. Systemic administration of C-type natriuretic peptide as a novel therapeutic strategy for skeletal dysplasias. Endocrinology 2009;150:3138–44.
[21] Bartels CF, Bukulmez H, Padayatti P, Rhee DK, van Ravenswaaij-Arts C, Pauli RM, et al. Mutations in the transmembrane natriuretic peptide receptor NPR-B impair skeletal growth and cause acromesomelic dysplasia, type Maroteaux. Am J Hum Genet 2004;75:27–34.
[22] Hachiya R, Ohashi Y, Kamei Y, Suganami T, Mochizuki H, Mitsui N, et al. Intact kinase homology domain of natriuretic peptide receptor-B is essential for skeletal development. J Clin Endocrinol Metab 2007;92:4009–14.
[23] Khan S, Hussain Ali R, Abbasi S, Nawaz M, Muhammad N, Ahmad W. Novel mutations in natriuretic peptide receptor-2 gene underlie acromesomelic dysplasia, type Maroteaux. BMC Med Genet 2012;13:44.
[24] Olney RC, Bukulmez H, Bartels CF, Prickett TC, Espiner EA, Potter LR, et al. Heterozygous mutations in natriuretic peptide receptor-B (NPR2) are associated with short stature. J Clin Endocrinol Metab 2006;91:1229–32.
[25] Bocciardi R, Ravazzolo R. C-type natriuretic peptide and overgrowth. Endocr Dev 2009;14:61–6.
[26] Moncla A, Missirian C, Cacciagli P, Balzamo E, Legeai-Mallet L, Jouve JL, et al. A cluster of translocation breakpoints in 2q37 is associated with overexpression of NPPC in patients with a similar overgrowth phenotype. Hum Mutat 2007;12:1183–8.
[27] Estrada K, Krawczak M, Schreiber S, van Duijn K, Stolk L, van Meurs JB, et al. A genome-wide association study of northwestern Europeans involves the C-type natriuretic peptide signaling pathway in the etiology of human height variation. Hum Mol Genet 2009;18:3516–24.
[28] Miura K, Namba N, Fujiwara M, Ohata Y, Ishida H, Kitaoka T, et al. An overgrowth disorder associated with excessive production of cGMP due to a gain-of-function mutation of the natriuretic peptide receptor 2 gene. PLoS One 2012;7:e42180.
[29] Potter LR, Hunter T. Identification and characterization of the major phosphorylation sites of the B-type natriuretic peptide receptor. J Biol Chem 1998;273:15533–9.
[30] Yoder AR, Robinson JW, Dickey DM, Andersland J, Rose BA, Stone MD, et al. A functional screen provides evidence for a conserved, regulatory, juxtamembrane phosphorylation site in guanylyl cyclase A and B. PLoS One 2012;7:e36747.
[31] Dickey DM, Burnett Jr JC, Potter LR. Novel bifunctional natriuretic peptides as potential therapeutics. J Biol Chem 2008;283:35003–9.
[32] Bryan PM, Potter LR. The atrial natriuretic peptide receptor (NPR-A/GC-A) is dephosphorylated by distinct microcystin-sensitive and magnesium-dependent protein phosphatases. J Biol Chem 2002;277:16041–7.
[33] Robinson JW, Potter LR. ATP potentiates competitive inhibition of guanylyl cyclase A and B by the staurosporine analog, Go6976: reciprocal regulation of ATP and GTP binding. J Biol Chem 2011;286:33841–4.
[34] Abbey-Hosch SE, Smirnov D, Potter LR. Differential regulation of NPR-B/GC-B by protein kinase C and calcium. Biochem Pharmacol 2005;70:686–94.

[35] Flora DR, Potter LR. Prolonged atrial natriuretic peptide exposure stimulates guanylyl cyclase-A degradation. Endocrinology 2010;151:2769–76.
[36] Fujishige K, Kotera J, Yanaka N, Akatsuka H, Omori K. Alteration of cGMP metabolism during chondrogenic differentiation of chondroprogenitor-like EC cells, ATDC5. Biochim Biophys Acta 1999;1452:219–27.
[37] Ivanova K, Heim JM, Gerzer R. Kinetic characterization of atrial natriuretic factor-sensitive particulate guanylate cyclase. Eur J Pharmacol 1990;189:317–26.
[38] Potter LR, Hunter T. Phosphorylation of the kinase homology domain is essential for activation of the A-type natriuretic peptide receptor. Mol Cell Biol 1998;18:2164–72.
[39] Chrisman TD, Garbers DL, Parks MA, Hardman JG. Characterization of particulate and soluble guanylate cyclases from rat lung. J Biol Chem 1975;250:374–81.
[40] Kimura H, Murad F. Evidence for two different forms of guanylate cyclase in rat heart. J Biol Chem 1974;249:6910–6.

RESEARCH ARTICLE

AMERICAN JOURNAL OF medical genetics PART A

Overgrowth Syndrome Associated With a Gain-of-Function Mutation of the Natriuretic Peptide Receptor 2 (*NPR2*) Gene

Kohji Miura,[1] Ok-Hwa Kim,[2] Hey Ran Lee,[3] Noriyuki Namba,[1] Toshimi Michigami,[4] Won Joon Yoo,[3] In Ho Choi,[3] Keiichi Ozono,[1] and Tae-Joon Cho[3]*

[1]Department of Pediatrics, Osaka University Graduate School of Medicine, Osaka, Japan

[2]Department of Radiology, Ajou University Hospital, Suwon, Republic of Korea

[3]Division of Pediatric Orthopaedics, Seoul National University Children's Hospital, Seoul, Republic of Korea

[4]Department of Bone and Mineral Research, Osaka Medical Centre and Research Institute for Maternal and Child Health, Osaka, Japan

Manuscript Received: 11 March 2013; Manuscript Accepted: 8 August 2013

The signal pathway of the C-type natriuretic (CNP) and its receptor, natriuretic peptide receptor 2 (NPR2) is involved in the longitudinal growth of long bones. Loss of function mutations at NPR2 cause acromesomelic dysplasia, type Maroteaux, while overproduction of CNP by chromosomal translocation and a gain-of-function mutation at NPR2 have been reported to be responsible for an overgrowth syndrome in three cases and one family, respectively. We identified a four-generation family with an overgrowth syndrome characterized by tall stature, macrodactyly of the great toes, scoliosis, coxa valga and slipped capital femoral epiphysis, similar to those previously reported in association with CNP/NPR2 overactivity. The serum level of amino-terminal proCNP was normal in the proband. A novel missense mutation of *NPR2*, c.1462G>C (p.Ala488Pro) was found to co-segregate with the phenotype in this family. In vitro transfection assay of the mutant NPR2 revealed overactivity of the mutant receptor at baseline as well as with the ligand. This overgrowth syndrome caused by a gain-of-function mutation at *NPR2* should be differentiated from Marfan or related syndromes, and may be categorized along with the overgrowth syndrome caused by overproduction of CNP due to its phenotypical similarity as overgrowth CNP/NPR2 signalopathy. © 2013 Wiley Periodicals, Inc.

Key words: tall stature; CNP signal; scoliosis; macrodactyly of the big toe; slipped capital femoral epiphysis

How to Cite this Article:
Miura K, Kim O-H, Lee HR, Namba N, Michigami T, Yoo WJ, Choi IH, Ozono K, Cho T-J. 2014. Overgrowth syndrome associated with a gain-of-function mutation of the natriuretic peptide receptor 2 (NPR2) gene.
Am J Med Genet Part A 164A:156–163.

INTRODUCTION

Natriuretic peptides are a family of hormones/paracrine factors regulating blood volume, blood pressure, ventricular hypertrophy, pulmonary hypertension, fat metabolism, and long bone growth [Potter et al., 2006]. They include atrial natriuretic peptide (ANP; OMIM 600296). CNP binds to a homodimeric transmembrane receptor, natriuretic peptide receptor B/guanylate cylcase B (NPR2; OMIM108961) to increase intracellular level of cyclic guanosine monophosphate (cGMP) [Schulz, 2005]. Several lines of evidence indicate that CNP-NPR2 signaling plays an important role in endochondral ossification [Yasoda et al., 1998; Teixeira et al., 2008]. Inactivation of CNP-NPR2 signaling resulted in dwarfism in both mouse and human. CNP knock-out mice ($Nppc^{-/-}$) or mice with homozygous loss-of-function mutations in *Npr2* result in undergrowth of the skeletal system [Chusho et al., 2001; Tsuji and Kunieda, 2005]. In humans, an autosomal recessive skeletal dysplasia, acromesomelic dysplasia, type Maroteaux (AMDM) characterized by disproportionately mesomelic shortening of the limbs and severe brachydactyly of the hands and feet is caused by homozygous or compound heterozygous loss-of-function mutations in *NPR2* [Bartels et al., 2004]. On the other hand, chronically elevated plasma level of CNP stimulates skeletal

Kohji Miura and Ok-Hwa Kim contributed equally to this work.

Grant sponsor: Ministry for Health, Welfare and Family Affairs Republic of Korea; Grant number: A080588; Grant sponsor: Ministry of Health, Labour and Welfare of Japan; Grant number: KH20Q007a-1.

*Correspondence to:
Tae-Joon Cho, M.D., Division of Pediatric Orthopaedics, Seoul National University Children's Hospital, 101 Daehang-ro Jongno-gu, Seoul 110-744, Republic of Korea.
E-mail: tjcho@snu.ac.kr

Article first published online in Wiley Online Library (wileyonlinelibrary.com): 20 November 2013
DOI 10.1002/ajmg.a.36218

growth in CNP-overproducing transgenic mice [Kake et al., 2009]. In humans, overproduction of CNP due to a chromosomal translocation causes an overgrowth syndrome [Bocciardi et al., 2007; Moncla et al., 2007]. A three-generation Japanese family was recently reported, with an overgrowth syndrome caused by a gain-of-function mutation in *NPR2* [Miura et al., 2012]. We identified and report a four-generation Korean family with similar phenotype and a novel gain-of-function mutation in *NPR2*.

MATERIALS AND METHODS

Clinical Report

This study was approved by the ethics committee at Seoul National University Hospital, and written informed consent was obtained from the proband and family members. An 8-year-old boy visited orthopedic clinic for awkward ambulation and ankle pain on walking. He was a product of normal full term pregnancy with a birth weight 3.2 kg and height 50 cm ($z = -0.04$). His macrodactyly of the big toe was observed since birth, something familiar to his family (Figs. 1 and 2). Developmental milestones were within normal limits. He was recognized as bigger than his age group after the neonatal period. On physical examination at 8 years of age, the height was 145 cm ($z = +3.67$), and weight was 40 kg (>97th centile). He had Marfanoid habitus and arachnodactyly. Neurologic examination was free of abnormal findings. At age 12 years, an unstable slipped capital femoral epiphysis (SCFE) developed on the left hip. Physical examination at this age revealed height 183 cm ($z = +5.19$), weight 71 kg (>97th centile), BMI 21.2 kg/m^2. He showed long and slender fingers and toes, the hallux being remarkably longer than the other toes, ankle valgus deformity, and scoliosis. No anomalies of cardiac valves or the aorta were found on echocardiogram. Blood pressure was within normal limits. No abnormality was observed in ophthalmic and otologic examinations. Hematological, biochemical and endocrinological values including insulin-like growth factor-I (IGF-I) were within normal ranges. However, bone formation and resorption markers were increased—osteocalcin, 118 ng/ml (reference range, 8–50); urinary cross-linked N-telopeptide of type I collagen, 969 BCE/mM creatinine (reference range, 21–83). Bone mineral density of L2-4 as measure by dual energy X-ray absorptiometry (Lunar Prodigy Advance, GE Healthcare, Waukesha, WI) was 0.791g/cm^2 ($z = -0.3$). Considering the tall stature of this patient, this BMD result may suggest presence of more severe osteopenia. Radiological survey of the skeleton showed coxa valga deformity of the femora, slipped capital femoral epiphysis, and lumbar scoliosis (Fig. 3). Arachnodactyly of all fingers and toes; of these, disproportionately long and large great toes were observed. Investigation of the family history revealed a four-generation family with 11 family members including the proband that could be considered to have the same phenotype. Five of 11 affected members were examined. They were characterized by tall stature (exceeded +4 SD compared to age matched control height of Korean population) and markedly long big toes. All of them showed coxa valga deformity with epiphyseal dysplasia of the femoral capital epiphyses and two had SCFE (Fig. 4). Three of them had lumbar scoliosis. The vertebral bodies were tall and showing endplate irregularities and narrowing of the intervertebral disc spaces in four of them. As seen in the clinical phenotype, radiograph of the feet showed extremely elongated metatarsals and assorted phalanges of the great toe symmetrically. The hands of all affected individuals showed arachnodactyly without elongation of specific fingers.

Mutation Analysis

Genomic DNA was extracted from the circulating leukocytes from the proband and family members available (Fig. 1). All the exons of *CNP*, *NPR2*, Natriuretic peptide receptor C (*NPR3*; MIM108962), and fibroblast growth factor receptor 3 (*FGFR3*; MIM134934) were

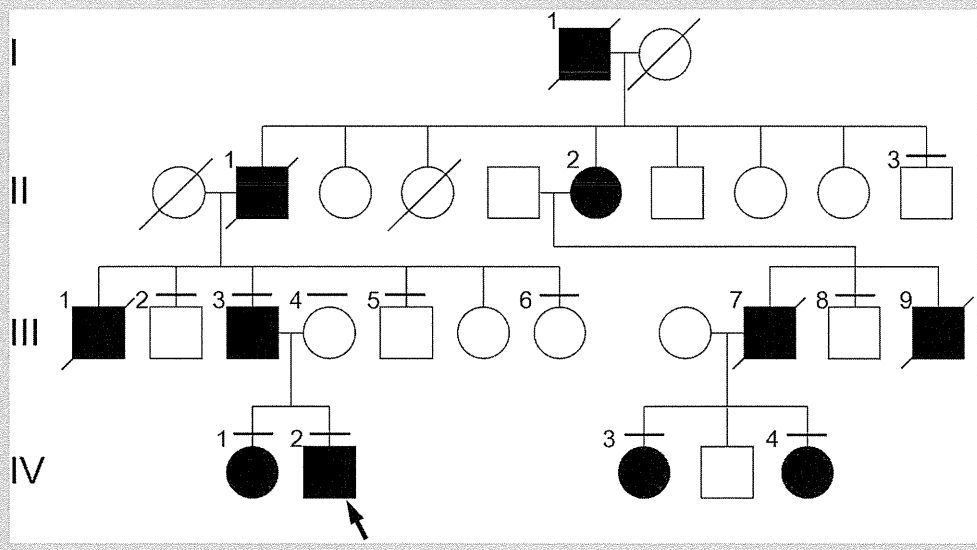

FIG. 1. Pedigree of the family. There are several father-to-son transmissions of the phenotype, revealing autosomal dominant inheritance pattern. Transverse bars above the circles or rectangles denote those who underwent mutation study. An arrow indicates the proband.

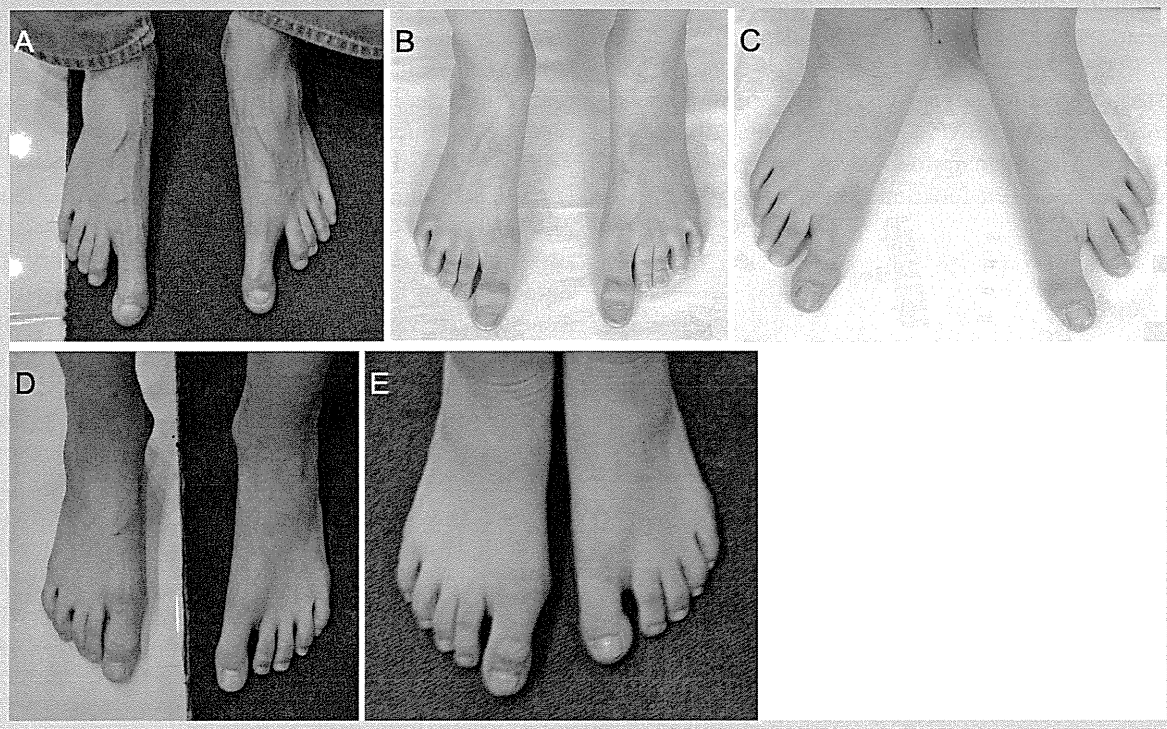

FIG. 2. Photographs of the feet of the affected family members. A: III-3, (B) IV-1, (C) IV-2, (D) IV-3, (E) IV-4. Patients IV-3 and IV-4 show relatively mild macrodactyly of the big toes as compared with the others.

amplified using specific primers [Miura et al., 2012] flanking the intron–exon boundaries according to published human genomic DNA sequences (UCSC genome browser: uc002vsl.1 at chromosome 2, 232498379–232499203; uc003zyd.1 at chromosome 9, 35782406–35799728; uc003jhv.2 at chromosome 5, 32711665–32787252; uc003gds.2 at chromosome 4, 1764337–1780396, respectively). Polymerase chain reaction (PCR) products was sequenced using a Big Dye terminator cycle sequencing kit (version 3.1; Applied Biosystems, Foster City, CA) and an ABI 3130 automated sequencer (Applied Biosystems).

Measurement of Serum Amino-Terminal (NT) proCNP Concentrations

Serum of IV-2 and III-3 were separated and collected, and NT-proCNP was assayed using an enzyme immunoassay (BIOMEDICA, Vienna, Austria) according to the instructions provided. As a control, samples from eight healthy Japanese teenager boys and five women were also measured.

In Vitro Transfection Assay of Mutant NPR2

The pcDNA3.1(+)/hemagglutinin (HA)-tagged human NPR2 wild-type vector (HA-WT) was a gift from Dr. Yoshihiro Ogawa (Tokyo Medical and Dental University, Japan) [Hachiya et al., 2007]. The construct encoding the mutant p.Ala488Pro, pcDNA3.1(+)/HA-human NPR-2 Ala488Pro (HA-Ala488Pro), was generated by PCR-based mutagenesis using HA-WT as the template, and primers containing the nucleotide change. All vector constructs were verified by bidirectional DNA sequencing.

HEK293A cells at confluence were transfected with empty vector containing green fluorescent protein(GFP), HA-WT, and HA-Ala488Pro using the liposomal transfection reagent FuGENE6 (Reagent: DNA = 3 μl: 0.5 μg, Roche, Indianapolis, IN, 12-well plate), according to the manufacturer's instructions. In 48 hr, cell lysate was harvested and immunoblot was performed to compare the expression of transfected genes, using a mouse monoclonal antibody against HA-tag (6E2, 1:1,000; Cell Signaling Technology, Boston, MA) as the primary antibody. As an internal control, β-actin in each sample was detected with a monoclonal anti-β-actin antibody (1:5,000; SIGMA-ALDRICH, Saint Louis, MO).

Transfected cells were serum-starved for 24 hr before the cGMP assay and then incubated at 37°C with 5% CO_2 in DMEM containing 0.5 mM IBMX (3-isobutyl-1-methylxanthine) (Wako, Osaka, Japan) for 10 min. The cells were next treated with vehicle (water) or 1×10^{-7} M CNP-22 (Biochem Life Sciences, New Delhi, India) and incubated for another 10 min. The reaction was terminated with 300 μl of 0.1 M HCl, and the cGMP concentration was measured by a competitive enzyme immunoassay (Cayman Chemical, Ann Arbor, MI). Results are presented as the mean ± SD. Student's *t* test was used for statistical analyses.

FIG. 3. Skeletal survey of the proband at age 12 years. A,B: Anteroposterior and lateral spine show lumbar scoliosis, slightly tall vertebral bodies with irregular end-plates, and narrowing of the intervertebral disc spaces. C: Pelvis shows coxa valga deformity and slipped femoral capital epiphysis on the left hip. D: Lower extremity demonstrates long and slender long bones with thin cortices. Mild inward bowing of the tibial and fibular diaphysis and ankle valgus deformity are noted. E: Feet show exceedingly long and large metatarsals and phalanges of the great toes symmetrically. F: Hands show overall arachnodactyly without specific digit elongation. Carpal bone age is advanced, measuring approximately 14 years of age.

RESULTS

Identification of a Novel Missense Mutation p.Ala488Pro in *NPR2*

On screening the sequences of exons of *CNP*, *NPR2*, *NPR3*, and *FGFR3* in the proband and family members as depicted on Figure 1, we identified a novel heterozygous sequence variation c. 1462G>C at *NPR2* in those who shared the similar phenotype (III-3, IV-1, IV-2, IV-3, and IV-4), but not in the remaining unaffected family members. The sequence variation eliminates an *Nhe*I cleavage site. PCR product of wild type containing this site (484 bp) would be cut into 95 and 389 bp fragments. Hence, these PCR products from all the patients tested were incubated with *Nhe*I (New England BioLabs, Ipswiich, MA) overnight and run on an agarose gel to confirm the presence of this sequence variation. It showed that this sequence variation perfectly co-segregated with the phenotype in this family. It was predicted to substitute alanine for proline (p. Ala488Pro). This variant was not registered in the dbSNP (build 137) (http://www.ncbi.nlm.nih.gov/projects/SNP/) nor in the NHLBI Exome Sequencing Project (ESP) (http://evs.gs.washington.edu/EVS/). It was not found in 400 alleles from healthy Korean or Japanese controls, either. Amino acid Ala488 is located in a highly conserved region of the juxtamembranous cytoplasmic domain of NPR2 and is conserved across species (Fig. 5). No mutations were found in *CNP*, *NPR3*, or *FGFR3*.

CNP Was Not Overproduced in the Proband

Serum NT-proCNP levels of the proband (IV-2) and his mother were measured 9.68 and 2.65 pmol/L, respectively. Those of eight Japanese teenager boys of age ranging from 12 to 14 years averaged 6.0 ± 3.4 pmol/L (mean ± standard deviation), and of five Japanese female adults of age ranging from 32 to 48 averaged 4.0 ± 0.9 pmol/L (unpublished data).

p.Ala488Pro Is a Gain-of-Function Mutation

To investigate the pathogenic significance of the p.Ala488Pro mutation, an in vitro functional assay was performed. HEK293A

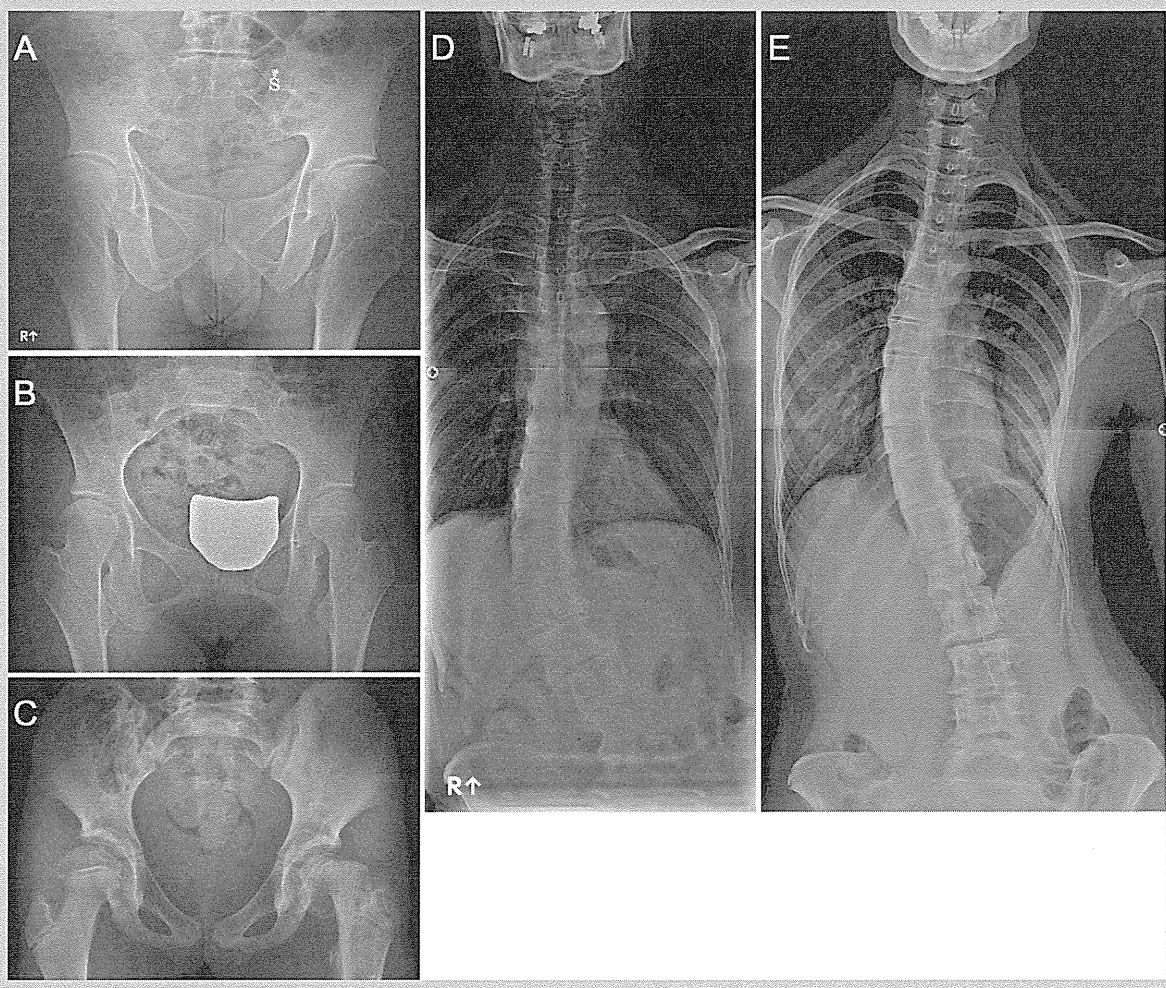

FIG. 4. Radiographs of the pelvis and spine of the other affected family members. Marked coxa valga deformity and residual valgus slipped capital femoral epiphysis are seen in Patients III-3 (A) and IV-1 (B). C: Coxa valga deformity and unstable aggravation of the slipped capital femoral epiphysis at the left hip are seen in Patient IV-3 at age 11 years. D: Patient III-3 and (E) Patient IV-1 show thoracolumbar scoliosis. The vertebral bodies are tall and narrowing of the disc spaces is noted.

cells were transfected with the GFP, HA-WT, and HA-Ala488Pro. The Western blot analysis using anti-HA antibody confirmed that HA-WT and HA-Ala488Pro were expressed at comparable levels, with an approximate molecular size of 120 kDa (Fig. 6A). cGMP production in the cells expressing HA-WT, and HA-Ala488Pro was also examined. cGMP was produced in Ala488Pro-expressing cells, even in the absence of CNP, while no production was observed in HA-WT-expressing cells. Treatment with CNP-22 at a dose of 1×10^{-7} M increased intracellular cGMP levels with concentrations significantly higher in HA-Ala488Pro than in HA-WT-expressing cells (Fig. 6B). These results indicate that p.Ala488Pro is a gain-of-function type mutation.

DISCUSSION

The CNP/NPR2 signal pathway is involved in the longitudinal growth of skeletal system [Yasoda et al., 1998; Chusho et al., 2001; Bartels et al., 2004; Tsuji and Kunieda, 2005; Bocciardi et al., 2007; Moncla et al., 2007; Teixeira et al., 2008; Kake et al., 2009]. Miura et al. [2012] reported a Japanese family with an overgrowth syndrome caused by a gain-of-function mutation at *NPR2*. The current study reports a second family showing a similar phenotype inherited as an autosomal dominant trait. The affected family members harbor a novel gain-of-function mutation at *NPR2*, c.1462G>C (p.Ala488Pro).

The mutation of the current family is located at a topological domain between transmembrane and protein kinase domainsrot[UniProtKB[Internet]], while the previously reported gain-of-function mutation was at the guanylate cyclase domain [Miura et al., 2012]. Although the current mutation does not exist at the guanylate cyclase domain, it must bring conformational change at the 3D structure of guanylate cyclase domain to enhance its enzymatic activity with or without binding the ligand.

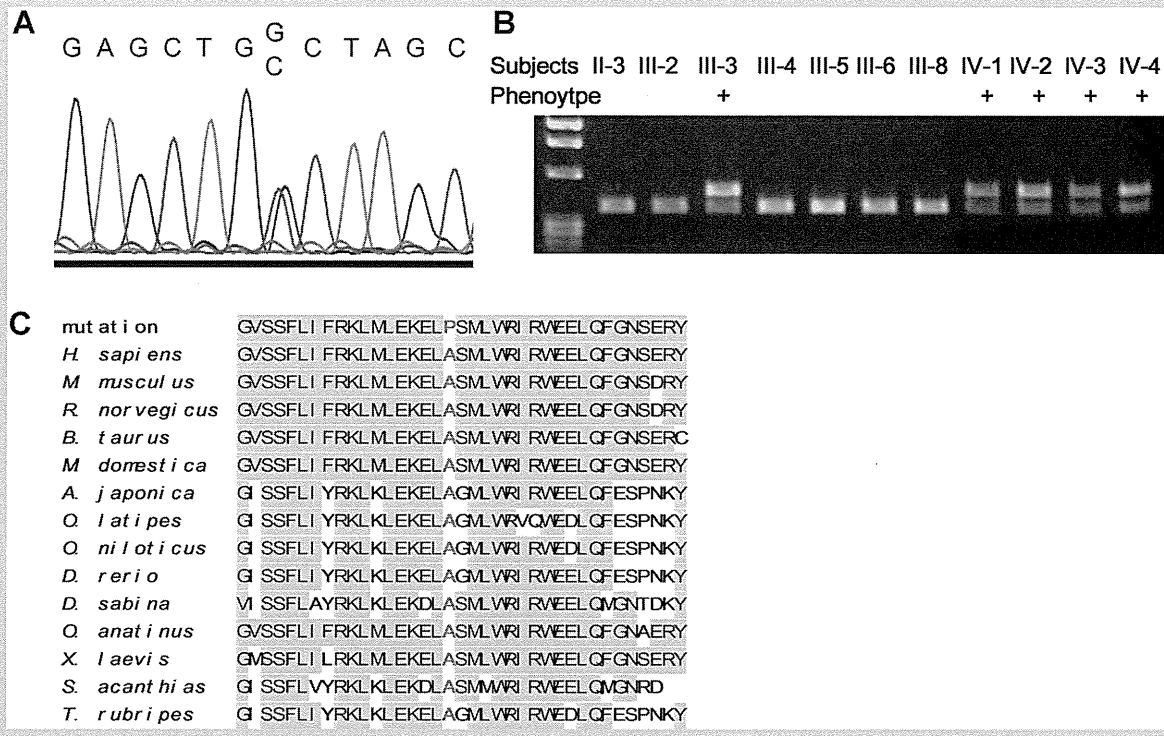

FIG. 5. Identification of the *Npr2* mutation. Sanger sequencing of the *NPR2* revealed a novel G → C missense mutation at nucleotide +1,462 creates a substitution, proline for alanine, at codon 488 in a heterozygous state. Among the subjects tested, this mutation was present in all the patients having the phenotype, and absent in all those who did not (A). This mutation eliminated the cleavage site of *Nhe*I, producing two bands on gel electrophoresis when treated with *Nhe*I (B). Amino acid alignment of NPR2 among various species. Alanine at codon 488 is located in a highly conserved cytoplasmic region between the transmembrane and protein kinase domains of NPR2 (C).

NPR2 is an interesting example of phenotypes contrasting between gain-of-function versus loss-of-function mutations at a gene encoding a receptor protein. Homozygous or compound heterozygous loss-of-function mutations of *NPR2* in humans cause a specific skeletal dysplasia, AMDM, characterized by marked short stature as well as short fingers and toes. The overgrowth syndrome by gain-of-function mutation seems to have phenotype opposite to that of AMDM. It is also interesting to note that the increased NPR2 activity did not suppress CNP production, maintaining its serum level within normal limit. The same unsuppressed CNP production was also observed in the previous cases of gain-of-function mutation at *NPR2* [Miura et al., 2012], suggesting lack of feedback loop between the NPR2 activity and CNP production.

This family has noticed 11 affected members by tall stature and long big toes through four generations. Neither macrodactyly of the big toe and ankle valgus deformity nor scoliosis and residual proximal femoral deformity of SCFE interferes with their daily living activities. One of them (IV-3) had even played basketball in a high school varsity team. However, development of unstable SCFE threatened function of the hip joint, and the proband was required to have major hip surgeries. SCFE is a chronic, gradual displacement of the femoral head at the proximal femoral physis. It may remain silent until physeal closure, and end up with residual deformity at the proximal femur as in the Patients III-3 and IV-1 (Fig. 4). However, in some cases, the SCFE could aggravate suddenly, resulting in unstable separation of the femoral head as in Patients IV-2 and IV-4 (Figs. 3 and 4), which is an orthopedic emergency requiring surgical intervention to stabilize the femoral head and to preserve its viability. Hence, once this disease entity is recognized, the patient should have an orthopedic consultation to monitor development and progress of SCFE, which was exclusively harbored by the affected members in this family. It is noteworthy that a residual deformity of silent SCFE showed posterolateral displacement of the femoral head (Fig. 4), a rare subtype of SCFE [Loder et al., 2006]. Scoliosis did not require any intervention in these affected family members. Macrodactyly of the big toes were not complained of in shoe fitting or cosmesis in the proband and affected family members.

The characteristic clinical and radiological findings make it a specific, discernible clinical disease entity, which can be differentiated from Marfan or other related syndromes. However, it is very similar to a phenotype caused by chromosomal translocation of 2q37 and subsequent CNP overproduction [Bocciardi et al., 2007; Moncla et al., 2007]. Hence, CNP overproduction and its receptor gene gain-of-function mutation may be categorized into a disease entity, that is, overgrowth CNP/NPR2 signalopathy, which should be included in differential diagnosis of the overgrowth syndrome.

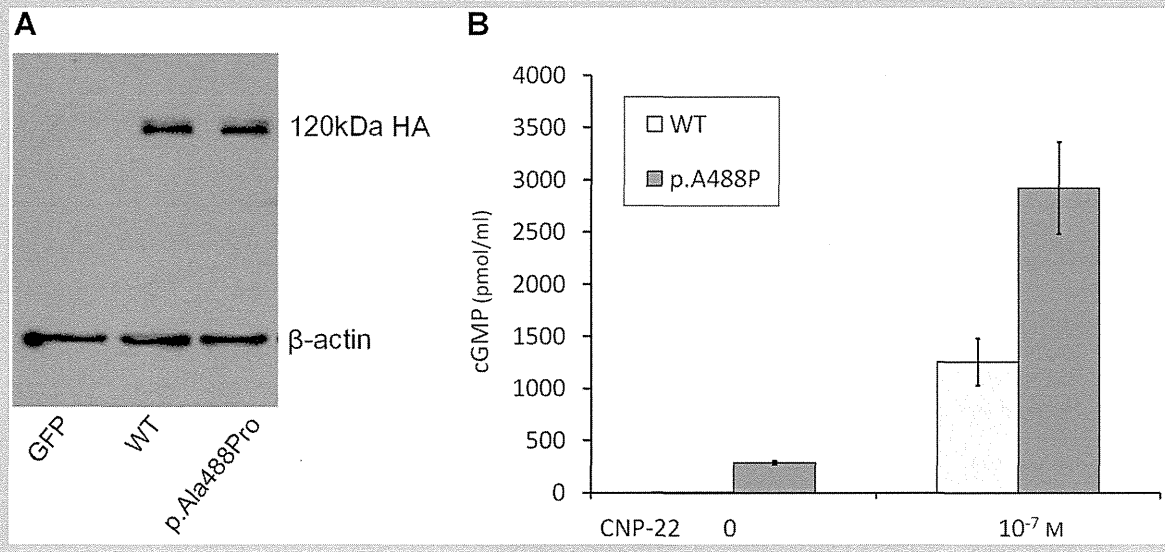

FIG. 6. NPR2 mutation of p.Ala488Pro is a gain-of-function mutation. A: Western blot analysis confirmed the comparable expression of HA-WT (WT) and HA-Ala488Pro. As an internal control, β-actin in each sample was detected with anti-β-actin antibody. B: Increased cGMP production in the HEK293A cells transfected with the p.Ala488Pro mutant compared to that in wild-type cells (WT). Forty-eight hours after the transfection, the cells were serum-starved for 24 hr, and then treated with the indicated concentrations of CNP-22 for 10 min, before cGMP production was assayed. Results are presented as the mean ± SD (N = 3, *$P < 0.05$).

In summary, we report on a family with an overgrowth syndrome inherited as autosomal dominant trait, which is caused by a gain-of-function mutation at *NPR2*. This is a distinct clinical entity that can be differentiated from other overgrowth syndromes by its clinical and radiological manifestations. Recognition of this specific disease entity will lead to targeted molecular study for confirmation, and will alert the clinician for potentially serious complication such as unstable SCFE.

ACKNOWLEDGMENTS

This study was supported in part by a grant from Ministry for Health, Welfare and Family Affairs, Republic of Korea (A080588) and in part by Grants-in-aid from the Ministry of Health, Labour and Welfare of Japan (KH20Q007a-1).

REFERENCES

Bartels CF, Bukulmez H, Padayatti P, Rhee DK, van Ravenswaaij-Arts C, Pauli RM, Mundlos S, Chitayat D, Shih LY, Al-Gazali LI, Kant S, Cole T, Morton J, Cormier-Daire V, Faivre L, Lees M, Kirk J, Mortier GR, Leroy J, Zabel B, Kim CA, Crow Y, Braverman NE, van den Akker F, Warman ML. 2004. Mutations in the transmembrane natriuretic peptide receptor NPR-B impair skeletal growth and cause acromesomelic dysplasia, type Maroteaux. Am J Hum Genet 75:27–34.

Bocciardi R, Giorda R, Buttgereit J, Gimelli S, Divizia MT, Beri S, Garofalo S, Tavella S, Lerone M, Zuffardi O, Bader M, Ravazzolo R, Gimelli G. 2007. Overexpression of the C-type natriuretic peptide (CNP) is associated with overgrowth and bone anomalies in an individual with balanced t(2;7) translocation. Hum Mutat 28:724–731.

Chusho H, Tamura N, Ogawa Y, Yasoda A, Suda M, Miyazawa T, Nakamura K, Nakao K, Kurihara T, Komatsu Y, Itoh H, Tanaka K, Saito Y, Katsuki M. 2001. Dwarfism and early death in mice lacking C-type natriuretic peptide. Proc Natl Acad Sci USA 98:4016–4021.

Hachiya R, Ohashi Y, Kamei Y, Suganami T, Mochizuki H, Mitsui N, Saitoh M, Sakuragi M, Nishimura G, Ohashi H, Hasegawa T, Ogawa Y. 2007. Intact kinase homology domain of natriuretic peptide receptor-B is essential for skeletal development. J Clin Endocrinol Metab 92:4009–4014.

Kake T, Kitamura H, Adachi Y, Yoshioka T, Watanabe T, Matsushita H, Fujii T, Kondo E, Tachibe T, Kawase Y, Jishage K, Yasoda A, Mukoyama M, Nakao K. 2009. Chronically elevated plasma C-type natriuretic peptide level stimulates skeletal growth in transgenic mice. Am J Physiol Endocrinol Metab 297:E1339–E1348.

Loder RT, O'Donnell PW, Didelot WP, Kayes KJ. 2006. Valgus slipped capital femoral epiphysis. J Pediatr Orthop 26:594–600.

Miura K, Namba N, Fujiwara M, Ohata Y, Ishida H, Kitaoka T, Kubota T, Hirai H, Higuchi C, Tsumaki N, Yoshikawa H, Sakai N, Michigami T, Ozono K. 2012. An overgrowth disorder associated with excessive production of cGMP due to a gain-of-function mutation of the natriuretic peptide receptor 2 gene. PLoS ONE 7:e42180.

Moncla A, Missirian C, Cacciagli P, Balzamo E, Legeai-Mallet L, Jouve JL, Chabrol B, Le Merrer M, Plessis G, Villard L, Philip N. 2007. A cluster of translocation breakpoints in 2q37 is associated with overexpression of NPPC in patients with a similar overgrowth phenotype. Hum Mutat 28:1183–1188.

Potter LR, Abbey-Hosch S, Dickey DM. 2006. Natriuretic peptides, their receptors, and cyclic guanosine monophosphate-dependent signaling functions. Endocr Rev 27:47–72.

Schulz S. 2005. C-type natriuretic peptide and guanylyl cyclase B receptor. Peptides 26:1024–1034.

Teixeira CC, Agoston H, Beier F. 2008. Nitric oxide, C-type natriuretic peptide and cGMP as regulators of endochondral ossification. Dev Biol 319:171–178.

Tsuji T, Kunieda T. 2005. A loss-of-function mutation in natriuretic peptide receptor 2 (Npr2) gene is responsible for disproportionate dwarfism in cn/cn mouse. J Biol Chem 280:14288–14292.

UniProtKB[Internet]. UniProt Consortium (EMBL-EBI, PIR, and SIB) [2002]. P20594(ANPRB_HUMAN) [updated January 9, 2013 Version 151, Cited January 12, 2013]. Available from http://www.uniprot.org/uniprot/P20594

Yasoda A, Ogawa Y, Suda M, Tamura N, Mori K, Sakuma Y, Chusho H, Shiota K, Tanaka K, Nakao K. 1998. Natriuretic peptide regulation of endochondral ossification. Evidence for possible roles of the C-type natriuretic peptide/guanylyl cyclase-B pathway. J Biol Chem 273: 11695–11700.

Journal of Neuroscience Research 00:00–00 (2014)

Primary Olfactory Mucosal Cells Promote Axonal Outgrowth in a Three-Dimensional Assay

Masahiro Ishihara, Noriko Mochizuki-Oda, Koichi Iwatsuki,* Haruhiko Kishima, Yu-ichiro Ohnishi, Takashi Moriwaki, Masao Umegaki, and Toshiki Yoshimine

Department of Neurosurgery, Osaka University Graduate School of Medicine, Suita City, Osaka, Japan

Among the possible sources of autologous cells and tissues for use in spinal cord injury grafts, one promising source is the olfactory mucosa containing olfactory ensheathing cells and neural progenitor cells. Olfactory mucosa transplantation for spinal cord injury has been effective in animal models and in pilot clinical trials. However, the contributions of olfactory ensheathing cells and neurons in olfactory mucosa are unclear. For the present study, we prepared primary olfactory mucosal cells and used a cortex–Matrigel coculture assay system to examine the axonal outgrowth of olfactory mucosa. Axonal outgrowth from cortical slices was significantly enhanced in olfactory mucosal cells compared with noncell controls and respiratory mucosal cells, which have few olfactory ensheathing cells and neurons. Axonal outgrowth was severely reduced after treatment with an antineurotrophin cocktail. A conditioned medium in the olfactory mucosa-derived cell group contained neurotrophin-3. Some olfactory ensheathing cells and almost all neurons were immunopositive for neurotrophin-3. Axons originating from cortical slices targeted mainly the astrocyte-like olfactory ensheathing cells. Our findings demonstrate that the axonal outgrowth effect of olfactory mucosa is supported by both olfactory ensheathing cells and neurons in olfactory mucosa.

Key words: neurite outgrowth; neural stem cells; neurotrophins

Despite major progress in medicine, developing effective treatment and rehabilitation strategies for spinal cord injury (SCI) remains a complex challenge. Spinal cord neurons have a limited regenerative capacity and are unable to regenerate after SCI because SCI provides an inhibitory environment (McDonald and Sadowsky, 2002). Several transplantation therapies have been surveyed for SCI in attempts to overcome this obstacle. Among the potential sources of autologous cells or tissues available for such transplantation therapies, the olfactory mucosa is the only nervous system tissue that is both capable and readily accessible with minimally invasive techniques (Winstead et al., 2005; Lima et al., 2006).

Olfactory mucosa, which is the main component of the mammalian olfactory system, has several distinct properties. In particular, olfactory mucosa is the only tissue that contains neurons with the capacity to grow and extend their axons directly into the central nervous system (CNS) throughout adulthood. The undifferentiated basal stem cells of the olfactory mucosa undergo a functional turnover throughout life, leading to a constant regeneration of olfactory sensory neurons (OSNs), sustentacular cells, and olfactory ensheathing cells (OECs). OECs are unique among glia in that they can migrate from the peripheral nervous system into the CNS. Together with the extending OSNs, OECs can migrate from the olfactory epithelium into the olfactory bulb. This unique property of the olfactory system is partially attributed to stem cells in the olfactory epithelium and to trophic and mechanical support provided by OECs that reside in the olfactory system (Mackay-Sim and St. John, 2011).

Whole-layer olfactory mucosa, which contains neural progenitor cells (NPCs) and OECs, also has been effective in SCI models (Lu et al., 2001, 2002; Iwatsuki et al., 2008, 2013b; Aoki et al., 2010). Therefore, autologous transplantation of olfactory mucosa has been undertaken in several clinics. Indeed, pilot studies have indicated that olfactory mucosa transplantation is effective for chronic, severe SCI (Lima et al., 2006, 2010; Chhabra et al., 2009; Iwatsuki et al., 2013a). These studies have emphasized that the neuroregenerative effects of olfactory mucosa might be attributable to OECs as well as NPC-derived neurons. However, the contributions of OECs and neurons remain unclear, even in animal SCI models (Iwatsuki et al., 2008; Aoki et al., 2010).

Additional Supporting Information may be found in the online version of this article.

Contract grant sponsor: Ministry of Education, Culture, Sports, Science, and Technology (Japan), contract grant number: 22791342.

*Correspondence to: Koichi Iwatsuki, Department of Neurosurgery, Osaka University Graduate School of Medicine, 2-2 Yamadaoka, Suita 565-0871, Japan. E-mail: kiwatsuki@nsurg.med.osaka-u.ac.jp

Received 15 November 2013; Revised 31 December 2013; Accepted 2 January 2014

Published online 00 Month 2014 in Wiley Online Library (wileyonlinelibrary.com). DOI: 10.1002/jnr.23367

The present study examines the axonal outgrowth of neurons and OECs residing in olfactory mucosa. To achieve this, we prepared primary olfactory mucosal cells and used a cortex–Matrigel coculture method (Ishihara et al., 2011) to quantify the axonal outgrowth of cortical motor neurons and cell–cell interactions between transplanted cells and axons in a three-dimensional culture. Finally, we evaluated these findings to determine the effectiveness of olfactory mucosa for regeneration after SCI.

MATERIALS AND METHODS

All animals were handled in accordance with the guidelines of the Laboratory Animals Care and Use Committee of the Osaka University Faculty of Medicine.

Primary Olfactory Mucosal Cells and Respiratory Mucosal Cells Cultures

Olfactory mucosal cells and respiratory mucosal cells were prepared as previously reported (Richter et al., 2008), with some modification. In brief, 8-week-old female Sprague-Dawley rats (Japan SLC Inc., Hamamatsu, Japan) were deeply anesthetized with sodium pentobarbital (100 mg/kg), and the nasal septum with attached olfactory mucosa and respiratory mucosa were dissected. Olfactory mucosa was taken from the most caudal end of the nasal septum. Respiratory mucosa was removed from the dorsal–anterior region of the septum. Olfactory mucosa and respiratory mucosa were minced with small surgical scissors, followed by a razor blade. The minced tissue was collected into Dulbecco's modified Eagle's/Ham's F12 medium (DMEM/F-12 Invitrogen, Carlsbad, CA). The suspension was spun at 170*g* for 10 min at room temperature (RT), aspirated, and then carefully triturated. The mixture was spun at 460*g* for 5 min at RT and then resuspended by trituration in the enzyme digestion mixture containing 1.2 mg/ml collagenase type I (Wako, Osaka, Japan), 1,800 PU/ml dispase II (Sanko, Kagawa, Japan) 15 μg/ml hydrouronidase (Sigma-Adrich, Munich, Germany), 100 U/ml DNase (Sigma-Adrich), and 1 mg/ml bovine serum albumin (BSA). The suspension was incubated for 60 min (for olfactory mucosa) or 30 min (for respiratory mucosa) in a water bath at 37°C with constant agitation at 100 oscillations/min. The suspension was spun at 460*g* for 5 min, and the supernatant was aspirated and triturated 35 times with a sterile Pasteur pipette that had been precoated with fetal bovine serum (FBS). Next, 10 ml of DMEM/F-12 was added to the tube. The digested tissue and the entire cell slurry were transferred through a 40-μm nylon cell strainer into a new conical tube. The collected cells were spun down at 460*g* for 5 min, and the supernatant was discarded. Cells were triturated in DMEM/F-12 with 10% FBS and 1% penicillin/streptomycin. The final concentration was 1.0×10^5 cells/ml. Cells were plated in 75-cm^2 flasks, and the flasks were incubated overnight at 37°C in 5% CO_2 to remove cell adhesion. On the next day, the floating cells were collected for use in the investigation.

Cortex–Matrigel Coculture and Axonal Outgrowth Assay

Cocultures of the brain cortex and a cell-suspended Matrigel (BD, San Jose, CA) were prepared as previously reported (Ishihara et al., 2011). Briefly, the cell suspension was mixed with the Matrigel in a 1:3 volume ratio, resulting in a final cell concentration of 1.0×10^6 cells/ml. Next, 10 μl of the suspended Matrigel was formed as a 6–7-mm × 4–5-mm rectangular shape on a cell culture insert. After incubating for 3 days, 400-μm thick sensorimotor cortex slices from day 3 postnatal SD rats were positioned along the long side of Matrigel (for detail see Supp. Info. Fig. 1). We used three culture groups: olfactory mucosal cells group, respiratory mucosal cells group, and no-cell control group (DMEM/F-12 with 10% FBS was also mixed with Matrigel at the same volume ratio). To confirm the composition and neurotrophin-producing ability of the olfactory mucosal cells and respiratory mucosal cells, we cultured Matrigel-containing olfactory mucosal cells or respiratory mucosal cells without a cortex slice. These cocultures were

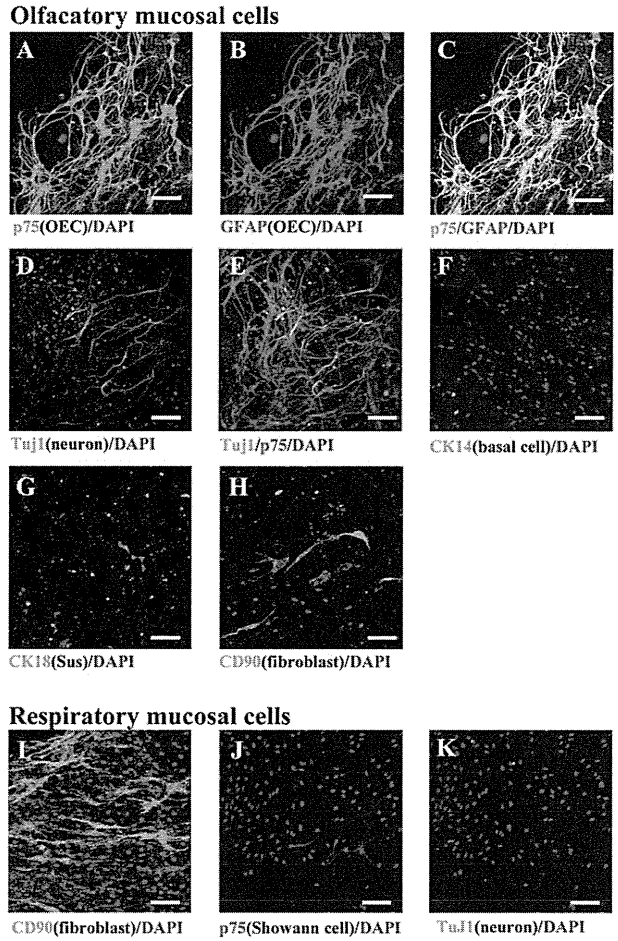

Fig. 1. Immunocytochemical characterization of olfactory mucosal cells (a–h) and respiratory mucosal cell (I–K) cultures. Immunofluorescence images of olfactory mucosal cells 10 days in vitro (DIV) stained by neuronal markers Tuj-1 (**D,E**). Nonneuronal cells were stained by p75 (**A,C,E**) and GFAP (**B,C**; OECs, olfactory ensheathing cells), CK14 (F, horizontal basal cells), CK18 (**G**, sustentacular cells), and CD90 (**H**, fibroblasts). Immunofluorescence images of respiratory mucosal cells (10 DIV) stained by CD90 (**I**, fibroblasts), p75 (**J**, suspected Schwann cells), and Tuj-1 (**K**, neural cells). Scale bars = 50 μm.

incubated in a humidified atmosphere with 5% CO_2 at 37°C for up to 7 days. Half of the medium was replaced every 3 days.

Quantitative analysis of axonal outgrowth and interactions between elongating axons and implanted cells were performed 7 days after coculture, as previously reported (Ishihara et al., 2011). In brief, fluorescence images were captured at a 2-μm pitch using a confocal laser microscope (Olympus FV-1000D). These pictures were projected over the Z-axis, and then merged manually in Olympus Fluoview Version 2.1c and Adobe Photoshop CS4 software. Axons passing through the reference lines and running parallel to the junction between the cortex and Matrigel at distances of 500, 1,000, 1,500, and 2,000 μm, were counted. To analyze cell-to-cell interactions, each one-third of an image was projected over the Z-axis. To examine how neurotrophic factors participated in axonal outgrowth, we added 10 μg neutralizing antibodies (final concentration 10 ng/ml) against brain-derived neurotrophic factor (BDNF), neurotrophin (NT)−3, NT-4/5, and nerve growth factor (NGF; antineurotrophin antibody sample pack 1; Millipore, Bedford, MA) into the cultured medium every 3 days. As a control, we added 10 μg nonspecific antibodies (negative control antibodies attached antineurotrophin antibody sample pack 1; Millipore) into the cultured medium every 3 days.

Immunohistochemistry

Cell-containing gels and the cocultured tissues were fixed on membranes for 1 hr in 4% paraformaldehyde at RT, penetrated by 0.6% Triton X-100 in phosphate-buffered saline (PBS) containing 1% BSA at RT for 30 min, blocked with blocking solution (10% normal goat serum [Sigma], 1.0% BSA, and 0.6% Triton X-100 in 0.1 M PBS) for 1 hr at RT, and then incubated overnight with primary antibodies in the blocking solution at 10°C. Antibodies directed against the following antigens were used to identify the different cell types present in the coculture system: βIII tubulin (Tuj-1; 1:100 rabbit polyclonal; Abcam, Cambridge, United Kingdom) for neurons, neurofilament-L (NF-L; 1:100 rabbit monoclonal; Cell Signaling Technology, Danvers, MA) for axons, glial fibrillary acidic protein (GFAP; 1:100 mouse monoclonal; Cell Signaling Technology) for astrocytes, p75 neurotrophin receptor (1:100 mouse polyclonal [Millipore] or 1:100 rabbit monoclonal [Abcam]) for OECs and Schwann cells, CD90 (1:50 mouse monoclonal; BD Pharmingen) for fibroblasts, cytokeratin-14 (CK-14; 1:100 mouse monoclonal; Abcam) for basal cells, cytokeratin-18 (CK-18; 1:100 mouse monoclonal; Abcam) for sustentacular cells and NT-3 (1:100 rabbit polyclonal; Abcam). On the following day, the tissues were further incubated with DyLight 488-conjugated goat anti-mouse antibodies (1:200) and DyLight 549-conjugated goat anti-rabbit antibodies (1:500) at 10°C for 3 hr. Finally, the tissues were counterstained with DAPI.

Enzyme-Linked Immunosorbent Assay

To confirm the neurotrophin-producing ability of olfactory mucosal cells and respiratory mucosal cells, the conditioned medium of olfactory mucosal cells, respiratory mucosal cells, and the no-cell control group was collected every 9 days in vitro, centrifuged, and frozen at −80°C until use. The protein analyses of conditioned medium were performed with an ELISA kit, following the manufacturer's instructions.

Statistical Analysis

The data were expressed as mean ± standard error of the mean (SEM). Statistical significance was determined with a Mann-Whitney U test with Bonferroni correction for multiple testing (cortex-Matrigel assay) or a Tukey-Kramer test (ELISA assay).

RESULTS

Immunohistochemical Characterization of the Olfactory Mucosal Cell and Respiratory Mucosal Cell Cultures

GFAP- and/or p75-positive cells accounted for 65.8% of olfactory mucosal cells and were thought to be OECs (Fig. 1A–C). These OECs showed either a bipolar Schwann cell-like or a flat astrocyte-like morphology. Tuj-1-positive cells accounted for 13.8% of the olfactory mucosal cells and were thought to be neurons (Fig. 1D); their axons ran along the OECs (Fig. 1E). CK-14-positive horizontal basal cells made up only 0.5% of the olfactory mucosal cells (Fig. 1F). CK-18-positive sustentacular cells also made up 0.5% of olfactory mucosal cells (Fig. 1G). CD90-positive fibroblasts were 4.6% of all olfactory mucosal cells (Fig. 1H). Unidentified cells were estimated to be 15% of the olfactory mucosal cells.

GFAP- and/or p75-positive cells accounted for 2.9% of all respiratory mucosal cells (Fig. 1J,K). Small numbers of trigeminal nerve axons innervate the respiratory mucosa (Schaefer et al., 2002). Therefore, GFAP/p75-positive cells in respiratory mucosal cells were considered Schwann cells. CD90-positive fibroblasts were the most prominent cell type among respiratory mucosal cells and were estimated to be 38.5% of all respiratory mucosal cells (Fig. 1I). Tuj-1-positive neurons, CK-14-positive basal cells, and CK-18-positive sustentacular cells were not identified among respiratory mucosal cells. Unidentified cells were estimated to be about 60% of respiratory mucosal cells. Olfactory mucosal cells contained OECs and neurons compared with respiratory mucosal cells, whereas respiratory mucosal cells contained fibroblasts compared with olfactory mucosal cells.

Axonal Outgrowth Induced by Olfactory Mucosal Cells and Respiratory Mucosal Cells

For the olfactory mucosal cell group ($n = 16$), the average numbers of labeled axons that extended 500 μm, 1,000 μm, 1,500 μm, and 2,000 μm past the junction were 179.6 ± 11.9, 106.0 ± 10.1, 66.3 ± 9.3, and 25.7 ± 6.0, respectively (Figs. 2A, 3). For the control group ($n = 16$), the average numbers of labeled axons that extended 500 μm, 1,000 μm, 1,500 μm, and 2,000 μm past the junction were 113.1 ± 10.2, 26.8 ± 7.6, 3.4 ± 1.6, and 0.7 ± 0.5, respectively (Figs. 2B, 3). For the respiratory mucosal cells group ($n = 16$), the average numbers of labeled axons that extended 500 μm, 1,000 μm, 1,500 μm, and 2,000 μm

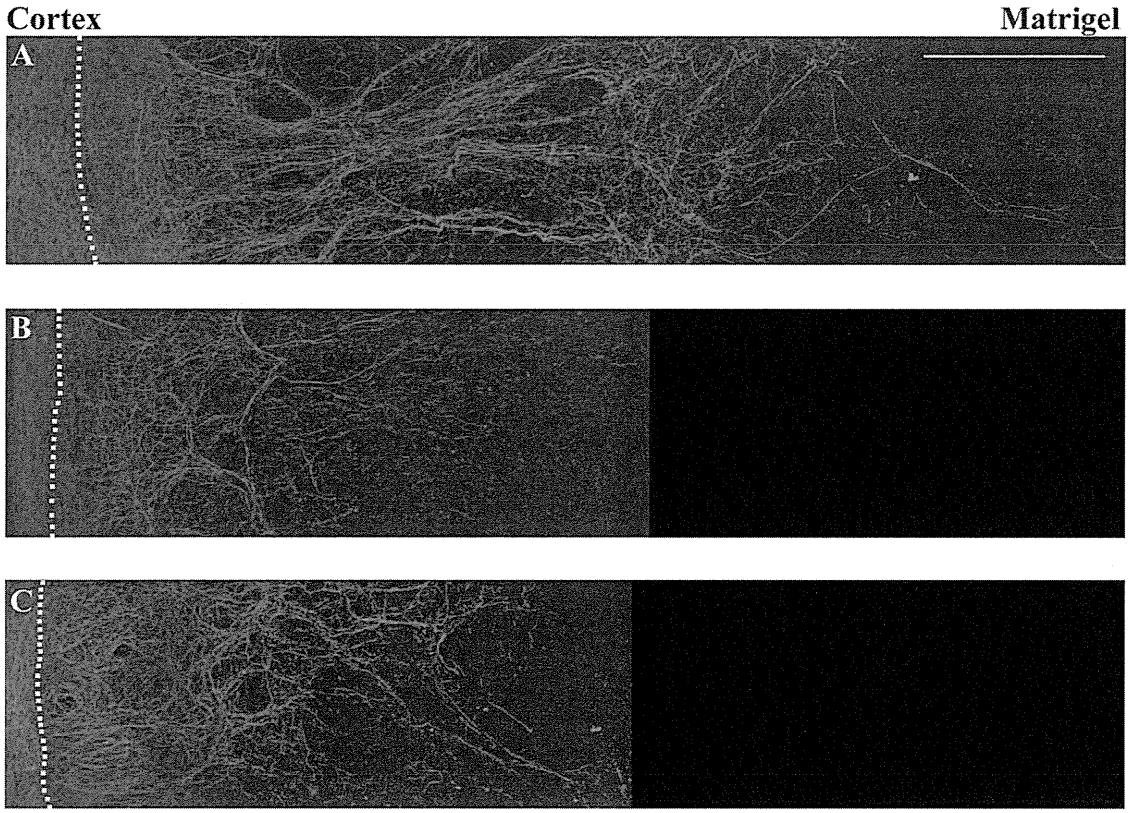

Fig. 2. Representative immunostaining images of axonal outgrowth 7 days after coculture using anti-NF-L antibody (red). **A:** Olfactory mucosal cells group. **B:** Controls (without cells). **C:** Respiratory mucosal cells groups. Dotted line indicates the border between the cortex and the Matrigel. Axonal outgrowth in the olfactory mucosal cells group was greater in number and length compared with that of the control or respiratory mucosal cells groups. Scale bar = 500 μm.

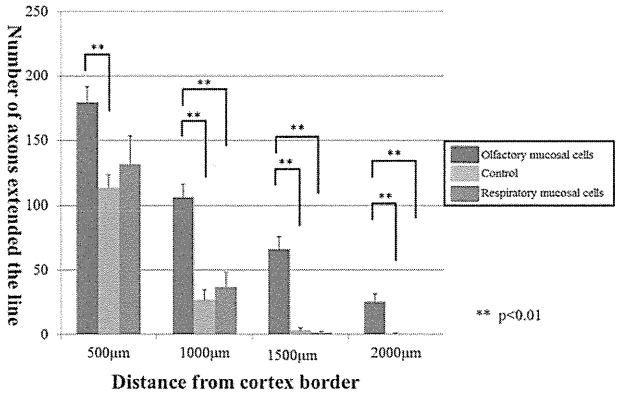

Fig. 3. Bar graph indicating axonal growth from the cortex to the Matrigel. The average number of axons in the olfactory mucosal cells group was significantly greater than that in the control group at distances of 500, 1,000, 1,500, and 2,000 μm from the junction. The average number of axons in the olfactory mucosal cells group was significantly greater than that in the respiratory mucosal cells group at distances of 1,000, 1,500, and 2,000 μm from the junction. The average number of axons was similar between control and respiratory mucosal cells groups. $^{**}P < 0.001$.

past the junction were 131.7 ± 21.6, 36.9 ± 11.3, 1.6 ± 0.9, and 0.0 ± 0.0, respectively (Figs. 2C, 3).

Axonal growth was significantly enhanced in the olfactory mucosal cells group for each distance compared with the control and for more than 1,000 μm compared with respiratory mucosal cells groups (Fig. 3). However, the respiratory mucosal cells group showed no axonal growth effect compared with the control group (Fig. 3).

Axonal Outgrowth Induced by Olfactory Mucosal Cells and Olfactory Mucosal Cells With Antineurotrophin Antibody Cocktails

For the olfactory mucosal cells with negative control antibodies (n = 6), the average numbers of labeled axons that extended 500 μm, 1,000 μm, 1,500 μm, and 2,000 μm past the junction were 277.3 ± 11.3, 162.3 ± 18.2, 76.0 ± 15.8, and 27.2 ± 12.8, respectively. For olfactory mucosal cells with antineurotrophins (n = 6), the average numbers of labeled axons that extended 500 μm, 1,000 μm, 1,500 μm, and 2,000 μm past the junction were 118.2 ± 18.2, 56.0 ± 9.9, 11.3 ± 2.6, and 0.0 ± 0.0, respectively. Axonal growth was significantly reduced in

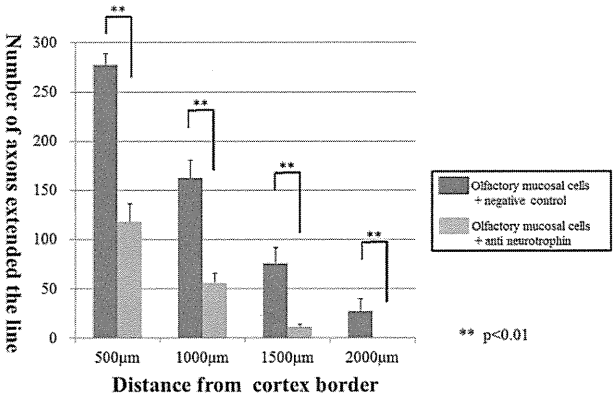

Fig. 4. Axonal outgrowth induced by olfactory mucosal cells with negative control antibodies and olfactory mucosal cells with antineurotrophin antibody cocktails. Olfactory mucosal cells with antineurotrophin cocktails showed significantly reduced axonal regeneration compared with olfactory mucosal cells in the negative control antibody groups. $^{**}P < 0.001$.

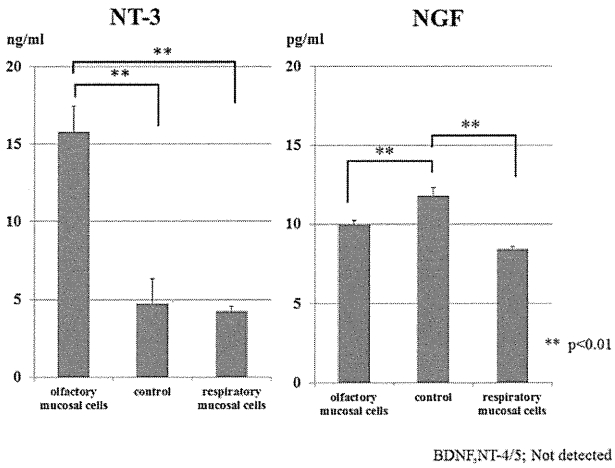

Fig. 5. Bar graph indicating neurotrophins in the conditioned medium. Olfactory mucosal cells produced larger amounts of neurotrophin (NT)−3 compared with control and respiratory mucosal cells; olfactory mucosal cells and respiratory mucosal cells consumed nerve growth factor (NGF) in the medium. $^{**}P < 0.001$.

olfactory mucosal cells in the presence of antineurotrophin (Fig. 4).

Neurotrophin Productivity Induced by Olfactory Mucosal Cells or Respiratory Mucosal Cells

The conditioned medium in olfactory mucosal cells contained 15.8 ± 1.7 ng/ml NT-3, whereas respiratory mucosal cells and controls contained 4.8 ± 1.6 ng/ml and 4.2 ± 0.3 ng/ml, respectively. NT-3 was significantly increased in olfactory mucosal cells compared with respiratory mucosal cells and controls. The conditioned medium in olfactory mucosal cells contained 9.9 ± 0.3 pg/ml NGF, whereas respiratory mucosal cells and controls contained 8.4 ± 0.1 pg/ml and 11.8 ± 0.5 pg/ml, respectively. NGF was decreased in olfactory mucosal cells and respiratory mucosal cells compared with controls. BDNF and NT-4 were below the deection limits in all groups (Fig. 5). Given the results in Figures 4 and 5, NT-3 is the key neurotrophin associated with axonal outgrowth in olfactory mucosal cells.

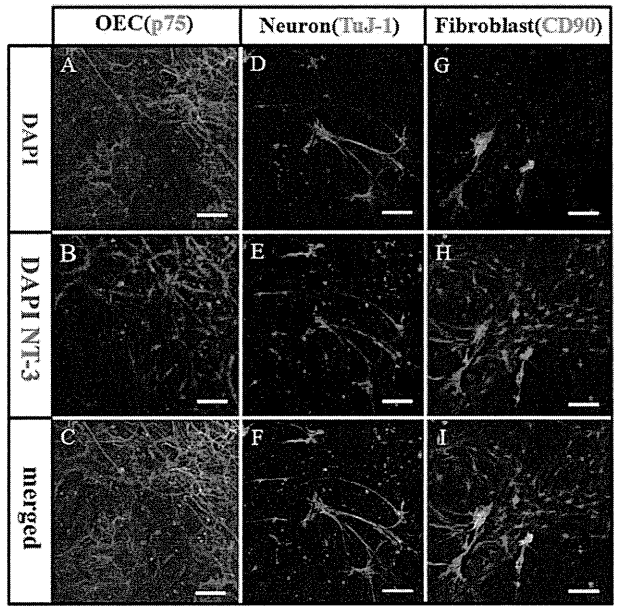

Fig. 6. Immunological staining of olfactory mucosal cells cultured for 7 DIV using p75 (green, **A,C**), Tuj-1 (green, **D,F**), CD90 (green, **G,I**), and NT-3 (red, **B,C,E,F,H,I**). Cell nuclei were counterstained with DAPI. NT-3-positive cells were mainly Tuj-1-positive neural cells; some olfactory ensheathing cells (OECs) were NT-3 positive. CD90-positive fibroblasts were positive for NT-3; however, the total number of NT-3-positive fibroblasts was small. Scale bars = 50 μm.

Immunohistological Identification of NT-3 Production in Olfactory Mucosal Cells

To detect which cell types contained NT-3, we performed NT-3 immunostaining for OECs, neurons, and fibroblasts, which were the top three components of olfactory mucosal cells (Fig. 1). P75-positive OECs, which were the primary component of olfactory mucosal cells, were partially positive for NT-3 (Fig. 6A–C). However, many NT-3-positive cells were not positive for p75 (Fig. 6C). Many Tuj-1-positive cells were positive for NT-3 (Fig. 6D–F). CD90-positive fibroblasts were positive for NT-3; however, we identified few fibroblasts (Figs. 1, 6G,I).

Interaction Between OECs and Growing Axons

Axons in the olfactory mucosal cells group tended to migrate into the surface area of the gel (Fig. 7). In the surface area of the gels, the axons grew in contact with

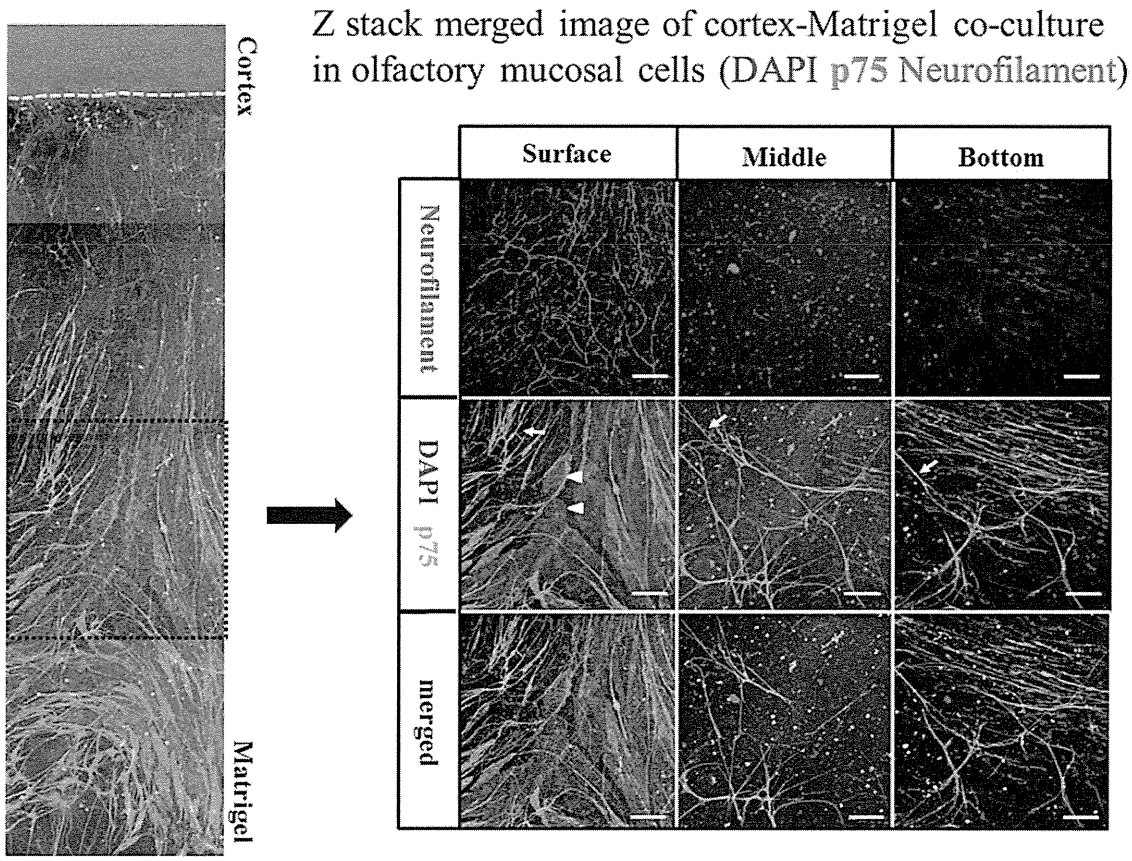

Fig. 7. Interactions between migrating axons and OECs in the Matrigel containing olfactory mucosal cells. Astrocyte-like OECs (arrowheads) were present mainly in the surface area of the gel. Regenerating axons from the cortex ran into the astroctyte-like OECs. In contrast, OECs were mainly Schwann cell-like shapes (arrow) in the middle and bottom of the gel, and axons scarcely existed in these areas. Scale bars = 50 μm.

the OECs (Fig. 7). OECs are known to show heterogeneity with two morphologies, Schwann cell-like or astrocyte-like phenotypes (Ekberg et al., 2012). Astrocyte-like OECs were found mainly in the surface area of the gel, whereas Schwann cell-like OECs were found in all areas of the gel. However, growing axons were attached mainly to astrocyte-like OECs, not Schwann cell-like OECs (Fig. 7).

DISCUSSION

Here we demonstrate that olfactory mucosal cells are rich in OECs and neurons compared with respiratory mucosal cells and that olfactory mucosal cells showed axonal outgrowth compared with respiratory mucosal cells and a no-cell control in a cortex–Matrigel coculture assay. Below we discuss axonal outgrowth induced in olfactory mucosal cells based on the three following points: 1) olfactory mucosal cells produced neurotrophins, 2) cell-to-cell interactions between elongating axons and olfactory mucosal cells, and 3) contribution by neurons in olfactory mucosal cells.

Neurotrophins Produced by Olfactory Mucosal Cells

In cultures, olfactory mucosal cells were composed mainly of OECs and neurons (Fig. 1). OECs and neurons in the olfactory mucosa have been reported to express neurotrophins (Buckland and Cunningham, 1999; Lipson et al., 2003; Feron et al., 2008). We added antineurotrophin antibody cocktail including anti-NT3, NT4/5, BDNF, and NGF in a cortex–Matrigel assay system to evaluate whether neurotrophins affected axonal regeneration. Olfactory mucosal cells treated with the antineurotrophin antibody cocktail drastically reduced their axonal outgrowth (Fig. 3). Given these results, we measured NT3, NT4/5, BDNF, and NGF concentrations in the conditioned medium of olfactory mucosal cells and found that NT-3 was abundant in olfactory mucosal cells but not in respiratory mucosal cells. Thus, NT-3 production is the key factor for promoting axon growth in olfactory mucosal cells.

NT-3 has been reported to support the survival and differentiation of neurons in the CNS (Conover and

Yancopoulos, 1997) and to stimulate corticomotor axon growth in an axon outgrowth assay with cortical slices (Oishi et al., 2004). NT-3 also has been described as a mitogen for OECs (Bianco et al., 2004). Therefore, NT-3 produced by olfactory mucosal cells was considered to stimulate axonal outgrowth for cortical neurons.

OECs express NGF, BDNF, GDNF, and CNTF (Buckland and Cunningham, 1999; Lipson et al., 2003); whether OECs express NT-3 or NT4/5 varies among studies. NT-3 mRNA was not detected in OECs (Boruch et al., 2001; Woodhall et al., 2001; Lipson et al., 2003), but immunoreactivity for NT-3 was observed in OECs (Liu et al., 2005). One report described detection of NT-4/5 mRNA in OECs (Boruch et al., 2001), whereas another study did not (Lipson et al., 2003). In our study, some OECs were immunopositive for NT-3, but many NT-3-positive cells were not immunopositive for p75 (Fig. 6C). Neurotrophin production and antigenicity of OECs appear to depend on the culture conditions (Pastrana et al., 2007; Huang et al., 2008; Novikova et al., 2011). Our culture medium was focused on the cortex slice and thus differed from typical OEC cultures. Therefore, the lack of NGF, BDNF, and NT-4/5 expression might be due to the culture conditions.

In our study, most neurons in olfactory mucosal cells were immunopositive for NT-3. From previous reports, OSNs are immunopositive for NT-3 (Feron et al., 2008), and, in transgenic NT-3 lacZ-neo mice, β-galactosidase is strongly expressed in a subset of OSNs, but not other types of cell in olfactory mucosa (Vigers et al., 2003). On the other hand, NT-3 mRNA was not detected in OECs (Boruch et al., 2001; Woodhall et al., 2001; Lipson et al., 2003), but immunoreactivity for NT-3 was observed in OECs (Liu et al., 2005). From these reports combined with our data, we speculated that OSNs produced NT-3 in the coculture system; by contrast, OECs might produce NT-3 or take up NT-3 and show immunogenicity for NT-3. Measurement of NT3 mRNA in each cell type was necessary for further survey, but isolation of OSNs was very difficult. Olfactory marker protein is the specific marker for OSNs; however, this maker is known not to be always positive for immature OSNs (Chen et al., 2008). On the other hand, several types of cells such as OECs were contaminated in primary OSNs culture (Gouadon et al., 2010). Therefore, we could not isolate OSNs and measure NT-3 mRNA in OSNs. This is a limitation of our study.

Cell-to-Cell Interactions Between Growing Axons and Olfactory Mucosal Cells

In our previous reports, we showed that axons from cortex in no-cell control groups run not only on the surface of the gel but also into the gels in this coculture system (Ishihara et al., 2011). In contact with olfactory mucosal cells, axons from cortex run mainly on the surface of the gel, in which astrocyte-like OECs are abundant. It is possible that axons and OECs both have a preference for the surface and that finding them together is coincidental. However, recent reports indicate that OEC migration regulates axon motility and stimulation of OEC motility enhances axonal extension (Windus et al., 2010) and that growth of olfactory axons in vitro was regulated predominantly by the motility of the underlying scaffold of OECs (Windus et al., 2011). Furthermore, olfactory mucosa affords a scaffold for axonal regeneration in rat SCI models (Iwatsuki et al., 2013b). Given these reports, we speculated that OECs in the gels provided a scaffold for axons from cortex.

Contribution by Neurons in Olfactory Mucosal Cells

Olfactory mucosa has long been known for its unique characteristic of generating neurons throughout adulthood. Olfactory mucosa contains OSNs and basal cells. Even though some reports indicated mesenchymal/ectmesenchymal stem cell in olfactory mucosa (Tome et al., 2009; Delorme et al., 2010), basal cells, especially horizontal basal cells, are reported to be neural stem cells (Murrell et al., 2005; Ohnishi et al., 2013). With methods to culture NSCs, basal cells can be grown in "neurosphere" cultures. This neurosphere of so-called olfactory stem cells can also generate not only OSNs but also other types of neurons such as dopaminergic neurons (Murrell et al., 2008), astrocytes, and oligodendrocytes (Roisen et al., 2001; Murrell et al., 2005). In our system, neurons in olfactory mucosal cells constituted about 13% of the total cell population (Fig. 1D) and horizontal basal cells were about 0.5% of the total cell population (Fig. 1F). Neurons in olfactory mucosal cells should differentiate into OSNs because we did not induce specific neurons or neural stem cells in the system, and some neurons in the gel were olfactory marker protein-positive, which is specific antigen for OSNs (data not shown). It was difficult to distinguish between neurons from olfactory mucosal cells and from cortical slices because olfactory marker protein is the marker for mature OSNs, and cultured neurons in olfactory mucosal cells are not always positive for olfactory marker protein (Chen et al., 2008).

In one study, strips of olfactory epithelium were grafted into the cortex, and fully developed OSNs were observed. Thus, axons from OSNs in olfactory epithelium grafts are capable of growing axons deep into the surrounding cortex and making synaptic connections with cortical neurons (Holbrook et al., 2001). The present study showed that transplanted neurons in olfactory mucosa could form connections with CNS neurons. Although we could not detect direct connections between neurons in olfactory mucosal cells and elongating axons from cortical slices, new neural circuits could be formed by neurons in olfactory mucosal cells. Our study at least suggests that neurons in olfactory mucosal cells contribute to the axonal outgrowth from the cortex by NT-3 production.

Recent pilot studies of olfactory mucosa autografts for chronic–complete SCI showed that motor evoked potentials or electromyography could be obtained in

some cases (Lima et al., 2010; Iwatsuki et al., 2013a). This means that new neural circuits from motor areas in the brain to muscles in lower extremities were formed. Previous reports on olfactory mucosa transplantation animal models showed that limited numbers of motor neurons were regenerated across the injured site (Iwatsuki et al., 2008; Aoki et al., 2010) and that olfactory mucosa afforded scaffolds for regenerating axons (Iwatsuki et al., 2013b). However, olfactory mucosal cells' contribution, especially neurons, is unknown. Our data demonstrate that olfactory mucosal cells' axonal outgrowth is promoted not only by OECs but also by neurons.

CONCLUSIONS

In this study, we demonstrate that olfactory mucosal cells show axonal outgrowth in a cortex–Matrigel coculture assay, but their axonal outgrowth ability was severely reduced by antineurotrophin cocktails. In combination with neurotrophin productivity of olfactory mucosal cells, NT-3 is thought to be a key factor for axonal outgrowth. Given the reports on the NT-3 productivity of OECs or OSNs and our data, we speculated NT-3 was produced mainly by neurons in olfactory mucosal cells. On the other hand, OECs provided scaffolds for outgrowth axons. Therefore, olfactory mucosal cells' axonal outgrowth ability was bestowed not only by OECs but also by neurons in olfactory mucosal cells.

ACKNOWLEDGMENTS

The authors thank Dr. Rieko Muramatsu from the Department of Molecular Neuroscience, Graduate School of Medicine, Osaka University, for technical advice.

REFERENCES

Aoki M, Kishima H, Yoshimura K, Ishihara M, Ueno M, Hata K, Yamashita T, Iwatsuki K, Yoshimine T. 2010. Limited functional recovery in rats with complete spinal cord injury after transplantation of whole-layer olfactory mucosa: laboratory investigation. J Neurosurg Spine 12:122–130.

Bianco JI, Perry C, Harkin DG, Mackay-Sim A, Feron F. 2004. Neurotrophin 3 promotes purification and proliferation of olfactory ensheathing cells from human nose. Glia 45:111–123.

Boruch AV, Conners JJ, Pipitone M, Deadwyler G, Storer PD, Devries GH, Jones KJ. 2001. Neurotrophic and migratory properties of an olfactory ensheathing cell line. Glia 33:225–229.

Buckland ME, Cunningham AM. 1999. Alterations in expression of the neurotrophic factors glial cell line-derived neurotrophic factor, ciliary neurotrophic factor and brain-derived neurotrophic factor, in the target-deprived olfactory neuroepithelium. Neuroscience 90:333–347.

Chen H, Dadsetan S, Fomina AF, Gong Q. 2008. Expressing exogenous functional odorant receptors in cultured olfactory sensory neurons. Neural Dev 3:22.

Chhabra HS, Lima C, Sachdeva S, Mittal A, Nigam V, Chaturvedi D, Arora M, Aggarwal A, Kapur R, Khan TA. 2009. Autologous olfactory [corrected] mucosal transplant in chronic spinal cord injury: an Indian pilot study. Spinal Cord 47:887–895.

Conover JC, Yancopoulos GD. 1997. Neurotrophin regulation of the developing nervous system: analyses of knockout mice. Rev Neurosci 8:13–27.

Delorme B, Nivet E, Gaillard J, Haupl T, Ringe J, Deveze A, Magnan J, Sohier J, Khrestchatisky M, Roman FS, Charbord P, Sensebe L, Layrolle P, Feron F. 2010. The human nose harbors a niche of olfactory ectomesenchymal stem cells displaying neurogenic and osteogenic properties. Stem Cells Dev 19:853–866.

Ekberg JA, Amaya D, Mackay-Sim A, St. John JA. 2012. The migration of olfactory ensheathing cells during development and regeneration. Neurosignals 20:147–158.

Feron F, Bianco J, Ferguson I, Mackay-Sim A. 2008. Neurotrophin expression in the adult olfactory epithelium. Brain Res 1196:13–21.

Gouadon E, Meunier N, Grebert D, Durieux D, Baly C, Salesse R, Caillol M, Congar P. 2010. Endothelin evokes distinct calcium transients in neuronal and non-neuronal cells of rat olfactory mucosa primary cultures. Neuroscience 165:584–600.

Holbrook EH, DiNardo LJ, Costanzo RM. 2001. Olfactory epithelium grafts in the cerebral cortex: an immunohistochemical analysis. Laryngoscope 111:1964–1969.

Huang ZH, Wang Y, Cao L, Su ZD, Zhu YL, Chen YZ, Yuan XB, He C. 2008. Migratory properties of cultured olfactory ensheathing cells by single-cell migration assay. Cell Res 18:479–490.

Ishihara M, Mochizuki-Oda N, Iwatsuki K, Kishima H, Iwamoto Y, Ohnishi Y, Umegaki M, Yoshimine T. 2011. A new three-dimensional axonal outgrowth assay for central nervous system regeneration. J Neurosci Methods 198:181–186.

Iwatsuki K, Yoshimine T, Kishima H, Aoki M, Yoshimura K, Ishihara M, Ohnishi Y, Lima C. 2008. Transplantation of olfactory mucosa following spinal cord injury promotes recovery in rats. Neuroreport 19: 1249–1252.

Iwatsuki K, Yoshimine T, Sankai Y, Tajima F, Umegaki M, Ohnishi Y, Ishihara M, Ninomiya K, Moriwaki T. 2013a. Involuntary muscle spasm expressed as motor evoked potential after olfactory mucosa autograft in patients with chronic spinal cord injury and complete paraplegia. J Biomed Sci Eng 6.

Iwatsuki K, Yoshimine T, Sankai Y, Umegaki M, Ohnishi Y, Ishihara M, Moriwaki T, Oda N. 2013b. Transplantation of olfactory mucosa as a scaffold for axonal regeneration following spinal cord contusion in rats. Neurosci Med 4:112–116.

Lima C, Pratas-Vital J, Escada P, Hasse-Ferreira A, Capucho C, Peduzzi JD. 2006. Olfactory mucosa autografts in human spinal cord injury: a pilot clinical study. J Spinal Cord Med 29:191–203; discussion 204–196.

Lima C, Escada P, Pratas-Vital J, Branco C, Arcangeli CA, Lazzeri G, Maia CA, Capucho C, Hasse-Ferreira A, Peduzzi JD. 2010. Olfactory mucosal autografts and rehabilitation for chronic traumatic spinal cord injury. Neurorehabil Neural Repair 24:10–22.

Lipson AC, Widenfalk J, Lindqvist E, Ebendal T, Olson L. 2003. Neurotrophic properties of olfactory ensheathing glia. Exp Neurol 180: 167–171.

Liu JB, Tang TS, Gong AH, Sheng WH, Yang JC. 2005. The mitosis and immunocytochemistry of olfactory ensheathing cells from nasal olfactory mucosa. Chinese J Traumatol 8:306–310.

Lu J, Feron F, Ho SM, Mackay-Sim A, Waite PM. 2001. Transplantation of nasal olfactory tissue promotes partial recovery in paraplegic adult rats. Brain Res 889:344–357.

Lu J, Feron F, Mackay-Sim A, Waite PM. 2002. Olfactory ensheathing cells promote locomotor recovery after delayed transplantation into transected spinal cord. Brain 125:14–21.

Mackay-Sim A, St John JA. 2011. Olfactory ensheathing cells from the nose: clinical application in human spinal cord injuries. Exp Neurol 229:174–180.

McDonald JW, Sadowsky C. 2002. Spinal-cord injury. Lancet 359: 417–425.

Murrell W, Feron F, Wetzig A, Cameron N, Splatt K, Bellette B, Bianco J, Perry C, Lee G, Mackay-Sim A. 2005. Multipotent stem cells from adult olfactory mucosa. Dev Dyn 233:496–515.

Murrell W, Wetzig A, Donnellan M, Feron F, Burne T, Meedeniya A, Kesby J, Bianco J, Perry C, Silburn P, Mackay-Sim A. 2008. Olfactory